Supplemental Information,

Aerosol filtration efficiency of household materials for homemade face masks: influence of material properties, particle size, particle electrical charge, face velocity, and leaks

Frank Drewnick[1], Julia Pikmann[1], Friederike Fachinger[1], Lasse Moormann[1], Fiona Sprang[1], Stephan Borrmann[1,2]

[1] *Particle Chemistry Department, Max Planck Institute for Chemistry, Mainz, Germany*
[2] *Institute for Atmospheric Physics, Johannes Gutenberg University, Mainz, Germany*

S1: Measurements and data analysis for the *CPC setup*

Prior to each measurement the setup was tested for potential leaks, especially around the seal of the sample, by introducing particle-free air and verifying that both CPCs measured zero particles per cm^3. Each particle transmission measurement was performed in two phases, both of them lasting for 30 s with CPC concentrations measured at 1-second time resolution using a self-written data acquisition software: during phase 1 CPC1 measured the particle number concentration upstream of the sample and CPC2 downstream of it. During phase 2 the two CPCs were swapped, in order to account for potential differences in counting efficiency of the two instruments. Since swapping the CPCs interrupts the flow and the concentrations, after every exchange of the CPCs it was waited until the concentrations had stabilized again before measurements were resumed. The transmission *T* of particles, i.e., the ratio of particle concentration behind to particle concentration in front of the filter sample, was calculated using the geometric mean of both measurement phases. *T* was determined from the measured particle concentrations according to

$$T = Corr \cdot \sqrt{\frac{\overline{CPC_2P_1}}{\overline{CPC_1P_1}} \cdot \frac{\overline{CPC_1P_2}}{\overline{CPC_2P_2}}}, \qquad [S1]$$

with $\overline{CPC_nP_m}$ the average concentration measured with CPC *n* (*n* = 1,2) during measurement phase *m* (*m* = 1,2). *Corr* is an experimentally determined correction factor (*Corr* = 0.99) for the overall transmission, which accounts for particle losses within the measurement setup when no sample is mounted.

The filtration efficiency *FE* (in percent) is determined from the transmission according to

$$FE = 100 \cdot (1 - T). \qquad [S2]$$

For each series of measurements the sample was freshly mounted into the test setup in order to account for potential variations in filtration efficiency due to differences in how the sample was fixed in the apparatus, e.g., due to different mechanical tension on the sample. A series of measurements included one measurement at each particle diameter (30 nm, 50 nm, 100 nm, 250 nm, and 500 nm) at a low pump flow rate (10 L min^{-1}) and a high flow rate (25 L min^{-1}) and with and without the additional neutralizer installed behind the DMA (see Fig. 1a), respectively. The measurements with the two different pump flow rates were performed to cover the typical range of average flow rates through a mask during regular breathing, albeit they do not attempt to mimic the human respiration cycle with up- and down-swelling flow rates and inversions of flow direction. Taking into account the additional flow rate of the CPC downstream the sample (F_{CPC} = 0.6 L min^{-1}) and the sample area, these two flow settings result in face velocities at the filter of 5.3 cm s^{-1} and 12.9 cm s^{-1}.

For calculation of average filtration efficiency, each measurement phase was divided into three intervals of 10 s. For each of these intervals *FE* was calculated individually, providing information on the temporal stability of the measurements. Each series of measurements (i.e., *FE* measurement for the various particle diameters and both face velocities) was repeated three times, resulting in a total of nine *FE* values for each material under each measurement condition. Values presented in the results section are averages of these nine values. Uncertainties are given as the 1-sigma standard deviation of the average.

S2: Measurement and data analysis for the *SMPS/OPC setup*

Each *FE* measurement started with approximately 5 minutes of equilibration time with the vacuum pump operating at the selected pump flow rate. Pump flow rates were adjusted for the slightly larger sample area and instrument flow rates in order to match the face velocities obtained in the CPC setup. When no temporal changes in aerosol concentrations downstream the sample were observed anymore, the filtration efficiency measurement was started. This measurement consisted of 20 minutes of simultaneous particle size distribution measurements of the ambient aerosol and the aerosol downstream of the sample, respectively, using the two OPCs in parallel. Data were collected with 6 s time resolution using a data acquisition computer with in-house developed software. In parallel, alternating measurements of the two aerosol size distributions were performed with the SMPS by manually switching between the two inlet lines (see Fig. 1b). During each *FE* measurement, three alternating 150-second scans for the ambient aerosol and for the aerosol downstream the sample, respectively, were performed. From these measurements three combinations of successive measurements were used to determine transmission efficiencies. The 20-minute interval of the OPC measurements was divided into three sub-intervals of approximately 7 min each; and every *FE* measurement was repeated three times with the sample being freshly mounted in the setup for each attempt. This procedure resulted in a total of nine ambient/downstream size distribution combinations (both for the OPCs and the SMPS) which were used to calculate average filtration efficiencies and the standard deviation of the average, used as uncertainty.

For calculation of filtration efficiencies, in a first step the measured concentrations of one of the OPCs was scaled to the other one to correct for differences in measurement efficiency of the two instruments and for the influence of the measurement setup. For this purpose, a particle-size dependent correction factor (range for individual size bins: factor 0.6-1.1) was applied, obtained from eight measurements on eight different days with both instruments and no filtering sample installed. The measured size distributions (dN / dlog d_p) were averaged over the respective measurement intervals and then re-binned from optical particle diameters into geometric particle diameters. For this conversion, we assumed a typical semi-urban size dependence of optical particle properties calculated from literature values (mixture of ammonium nitrate, ammonium sulfate, ammonium chloride, and organics, all with refractive indices of or close to 1.55 (Tang, 1996;Levin et al., 2010), in the smaller size range (d_p<700 nm), and of mineral dust (1.56-i0.006; Seinfeld and Pandis, 2006) in the larger size range (d_p>3000 nm), and a log-linearly interpolated mixture (by particle number) of the two particle types in the intermediate size range). A scattering angle of 60° to 120°, a wavelength of 655 nm, and a refractive index of 1.588 of calibration particles (PSL) (based on information from the manufacturer) and a distance of scattering volume to detector of 1.5 cm (Vetter, 2004) were assumed for these calculations; by these means, Mie scattering curves for calibration particles and for accumulation mode / mineral dust particles were calculated using an in-house developed software tool (Vetter, 2004) and the particles were re-assigned accordingly from optical to geometric diameter. From these number size distributions, filtration efficiencies as a function of particle size d_p were calculated according to

$$FE(d_p)[\%] = \left(1 - \frac{\overline{\frac{dN}{dlog\ d_{p,downstream}}}}{\overline{\frac{dN}{dlog\ d_{p,ambient}}}}\right) \cdot 100 = \left(1 - \frac{\overline{C_{downstream}(d_p)}}{\overline{C_{ambient}(d_p)}}\right) \cdot 100\,, \qquad \text{[S3]}$$

with $\overline{\frac{dN}{dlog\ d_{p,downstr./ambient}}}$ the average number size distribution and $\overline{C_{downstream/ambient}(d_p)}$ the average particle-size dependent concentration measured downstream or in ambient air.

From the consecutive ambient/downstream SMPS measurements, filtration efficiencies were calculated in the same way (Eq. S3). To reduce noise and to obtain similar bin sizes as for the OPC data, the *FE* values of typically four SMPS size bins were averaged.

Finally, the size dependent filtration efficiencies obtained with OPC and SMPS measurements were merged by averaging data from both instruments for the overlap particle size range from 250 nm up to 350 nm including 10 SMPS and 2 OPC size bins. The OPC and SMPS filtration efficiency curves agreed in this particle size range within typically less than 10%. Filtration efficiencies for the desired particle sizes (30 nm, 50 nm, 100 nm, 250 nm, 500 nm, 1 µm, 2.5 µm, 5 µm, and 10 µm) were calculated from the merged *FE* distributions using a running mean (3-9 points, depending on noise level), followed by a smoothing spline with estimated standard deviation of the noise of the data.

Especially for the largest particle sizes, particle number concentrations are relatively low. Therefore, in addition to the standard deviation, also the uncertainty due to counting statistics was calculated for each particle size, using the number of particles measured in the respective size bins. Provided in the results section are always the larger of the two uncertainty values.

Table S1: Overview of all measured samples. Note that in the summary figures Cotton, Jersey, Muslin, and Poly are presented both as single and double layered sample. For ready-made masks, area density is given for the respective stack of textiles; area density for all other samples as well as all thread counts are provided per layer of material.

Sample/Mask	**Short name**	**Composition**	**Area density / g m^{-2}**	**Thread count / thread number inch^{-2}**	**Comment**
Pure cotton fabric					
Cotton woven	Cotton	100% cotton	139	117	1-5 layers of fabric
Cotton jersey	Jersey	100% cotton	265	140	1-5 layers of fabric
Cotton shirt fabric	CottonShirt	100% cotton	128	178	Two layers of fabric
Cotton twill	CottonTwill	100% cotton	196	114	
Molleton	Molleton	100% cotton	182	80	1-5 layers of fabric, fabric washed several times
Muslin	Muslin	100% cotton	143	121	Two layers of fabric
Velvet cotton	VelvetCotton	100% cotton	288	164	
Dish towel	DishTowel	100% cotton	265	76	Two layers of fabric, washed several times
Surgical gown mask	SurgicalGown	100% cotton	513	130	Mask with two layers of fabric
Poplin mask 1	Poplin1	100% cotton	639	-	Mask with two layers of cotton shirt fabric and one layer of poplin fabric
Poplin mask 2	Poplin2	100% cotton	643	217	Mask with two layers of poplin fabric
Poplin mask 3	Poplin3	100% cotton	676	-	Mask with two layers of dense cotton fabric and one layer of poplin fabric
Cotton & synthetic mixed fabric					
Flannel	Flannel	Cotton, synthetic fiber	524	109	
French terry	FrenchTerry	Cotton, synthetic fiber	282	88	Two layers of fabric
Velour	Velour	80% cotton, 20% polyester	241	95	Two layers of fabric
Tennis socks mask	TennisSocks	85% cotton, 10% polyamide, 5% elastane	717	55	Mask with two layers of fabric
Surgical selfmade mask	SurgMaskSelfmade	100% cotton (outer layers), 100% synthetic fiber (inner layers)	284	-	Sample with two layers of cotton fabric and four layers of gauze (non-woven sheet) in between

Synthetic fibers					
Polyester	Poly	100% polyester	213	-	1-5 layers of fabric
Micro polyester	MicroPoly	100% polyester	203	-	
Polyester + elastane	PolyEla	91% polyester, 9% elastane	245	91	
Velvet polyester	VelvetPoly	100% polyester	291	137	Two layers of fabric
Viscose jersey	ViscoseJersey	100% viscose	213	114	Two layers of fabric
Viscose woven	Viscose	100% viscose	167	151	Two layers of fabric
Felt	Felt	Synthetic fiber	708	-	Thickness: 3.5 mm
Fleece	Fleece	100% polyester	243	-	Two layers of fabric
Microfiber terry	MicrofiberTerry	100% microfiber	292	-	
Microfiber	Microfiber	100% microfiber	122	-	
Swimsuit	Swimsuit	Synthetic fiber	288	150	Mask with two layers of fabric
Natural fibers					
Linen	Linen	100% linen	215	79	Two layers of fabric
Silk	Silk	100% silk	87	210	
Thin silk	SilkThin	100% silk	64	239	Two layers of fabric
Wool	Wool	100% wool	238	63	
Paper-like materials					
Paper towel 1	PaperTowel1	Paper/cellulose	55	-	Two layers of material
Paper towel 2	PaperTowel2	Paper/cellulose	40	-	Two layers of material
Tissue	Tissue	Paper/cellulose	52	-	
Coffee filter	CoffeeFilter	Paper/cellulose	53	-	
Other synthetic household materials					
Encasement 1	Encase1	70% polyester, 30% polyamide	621	-	Two layers of mattress encasement material, washed once, used as hypo-allergenic bedding
Encasement 2	Encase2	100% polypropylene	69	-	Used as hypo-allergenic bedding
Vacuum cleaner bag backup filter	VacBackup		127	-	Filter between vacuum cleaner bag and vacuum cleaner blower
Vacuum cleaner bag 1	VacBag		99	-	
Vacuum cleaner bag 2	VacBag2		129	-	
PU foam	PU	100% polyurethane	142	-	Punched out mask, thickness: 5.4 mm
PU filter foam	PU2	100% polyurethane	283	-	Punched out mask, thickness: 2 mm
Triangle bandage	TriangleBandage	Synthetic fiber	81	-	Non-woven fabric, two layers of fabric

Medical masks				
Surgical mask 1	SurgicalMask1	63	-	Several layers of non-woven material
Surgical mask 2	SurgicalMask2	78	-	Several layers of non-woven material
Surgical mask 3	SurgicalMask3	90	-	Several layers of non-woven material
Surgical mask 4	SurgicalMask4	104	-	Several layers of non-woven material; used for leak measurements only
FFP2 respirator	FFP2	172	-	Several layers of non-woven material; fold-up design

112

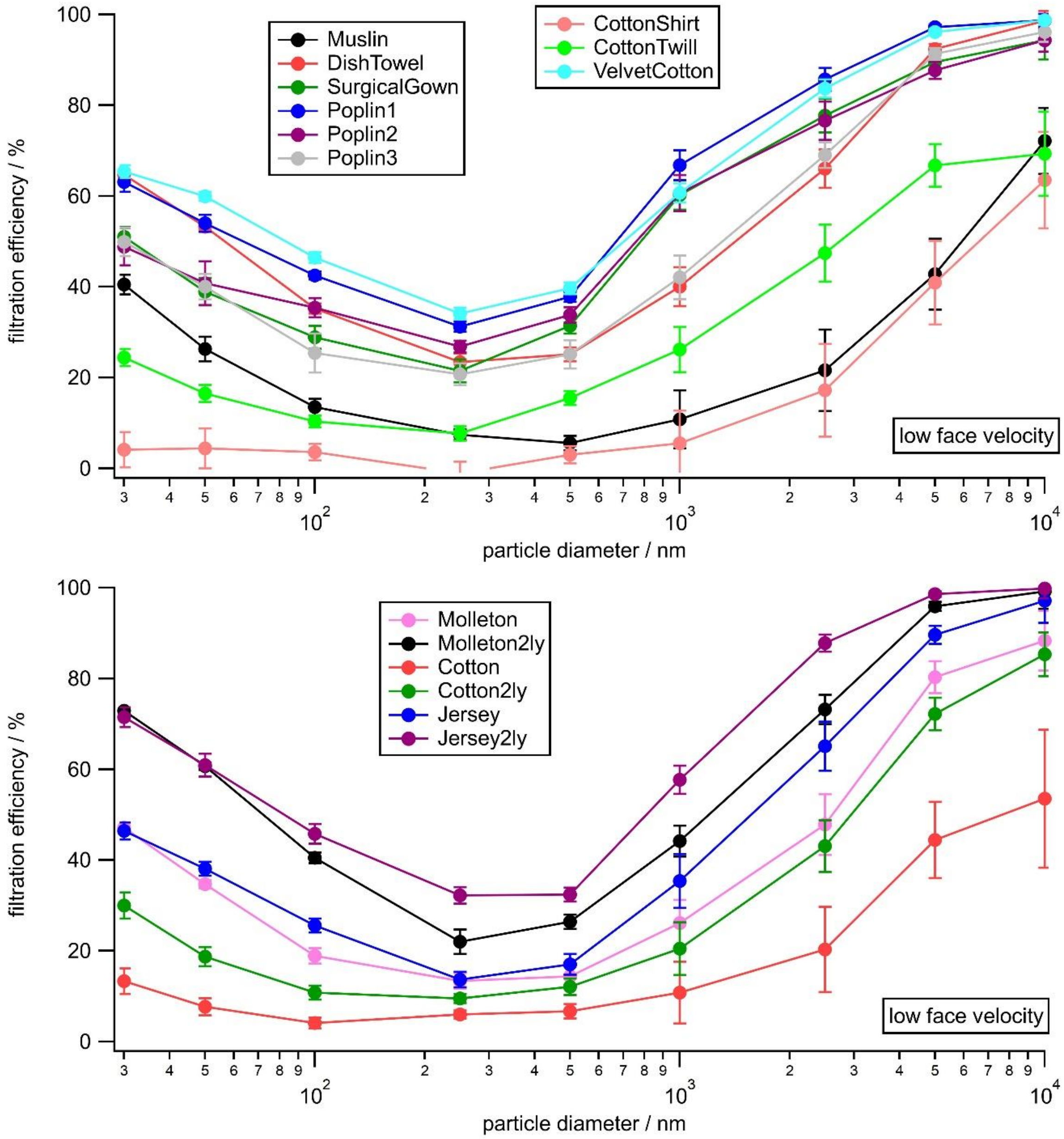

Figure S1a: Size-dependent filtration efficiency (ambient aerosol, measured with the *SMPS/OPC setup*, low face velocity) for “pure cotton fabric” materials.

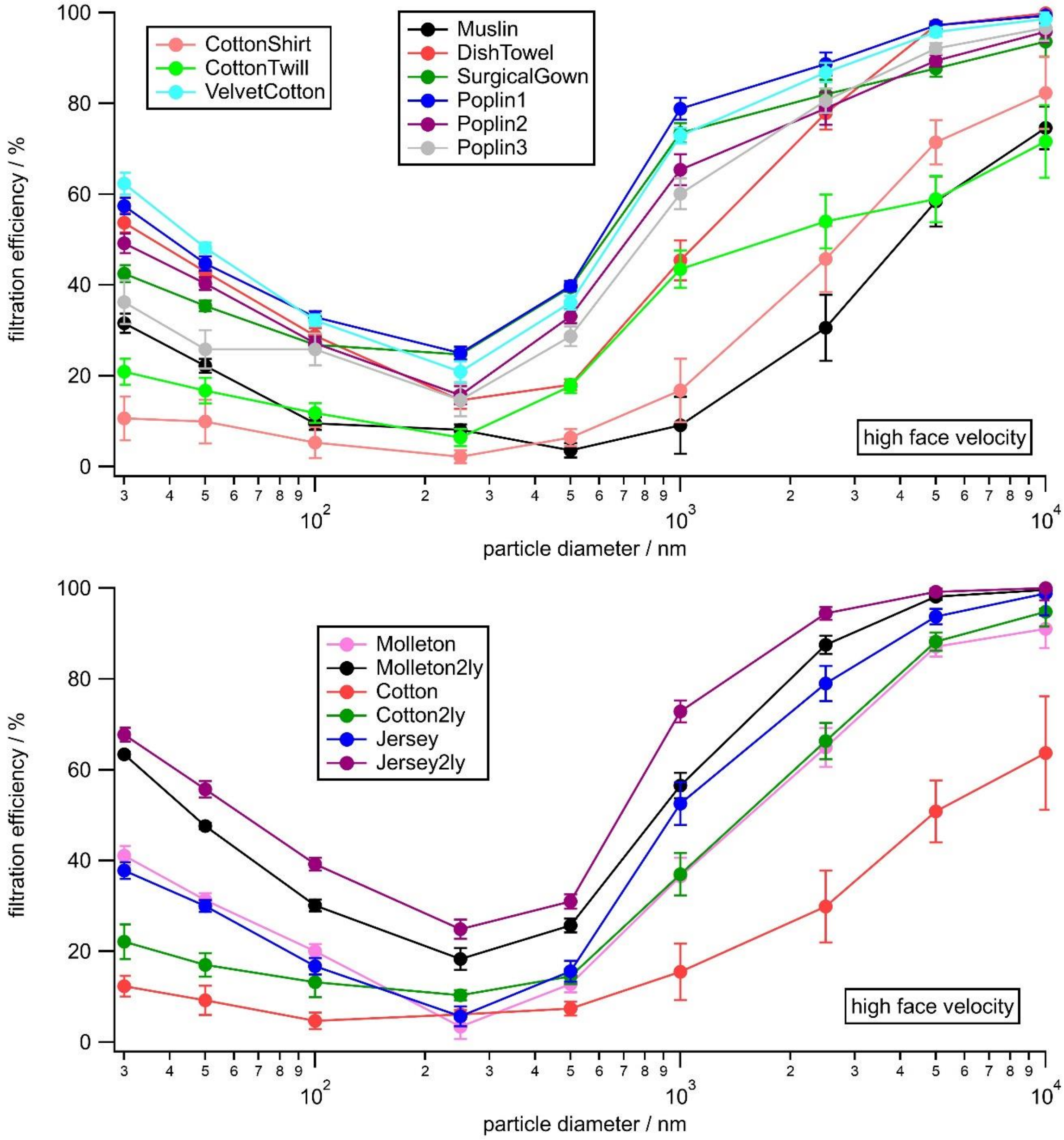

Figure S1b: Size-dependent filtration efficiency (ambient aerosol, measured with the *SMPS/OPC setup*, high face velocity) for “pure cotton fabric” materials.

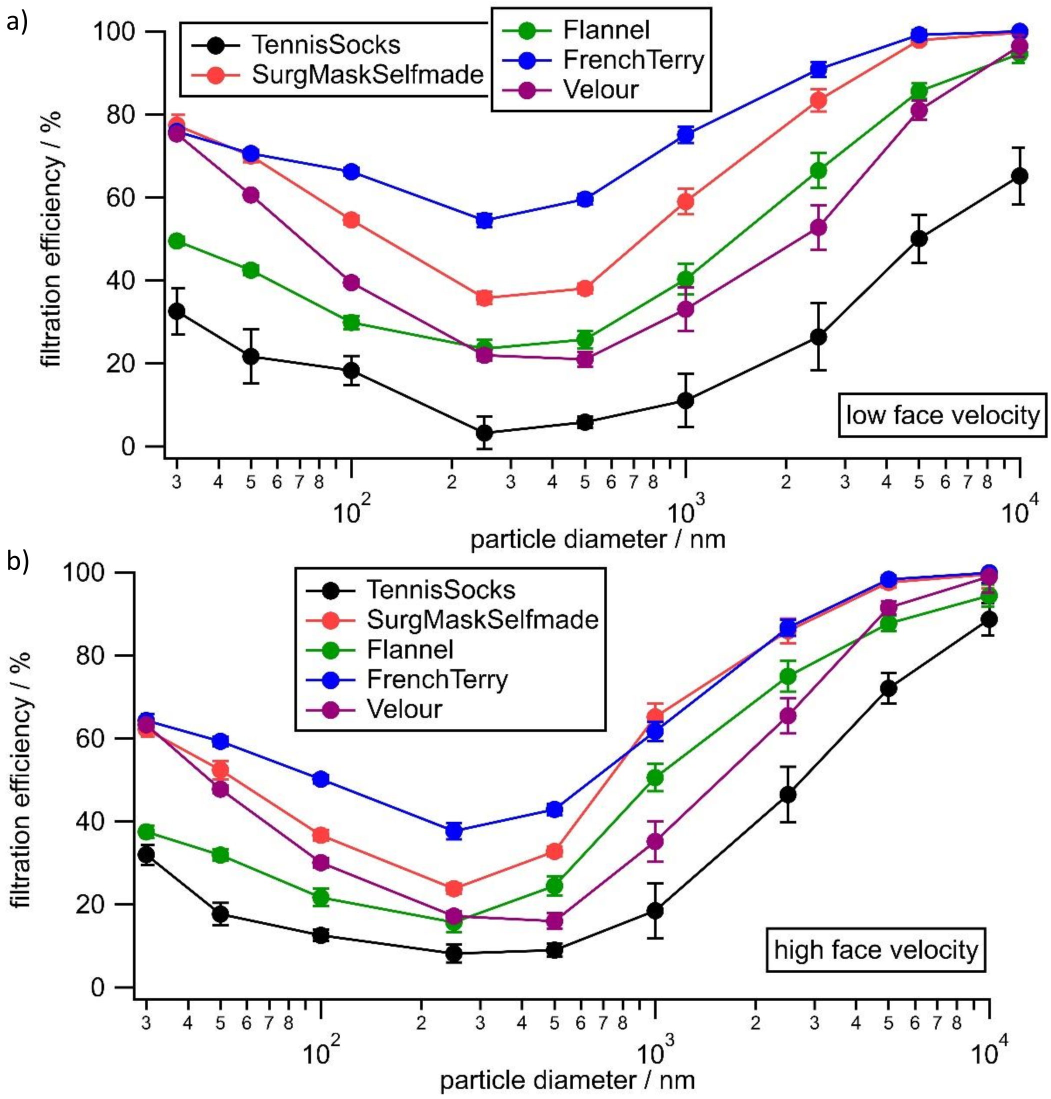

Figure S2: Size-dependent filtration efficiency (ambient aerosol, measured with the *SMPS/OPC setup*) for “cotton and synthetic mixed fabric” materials, measured at a) low and b) high face velocity.

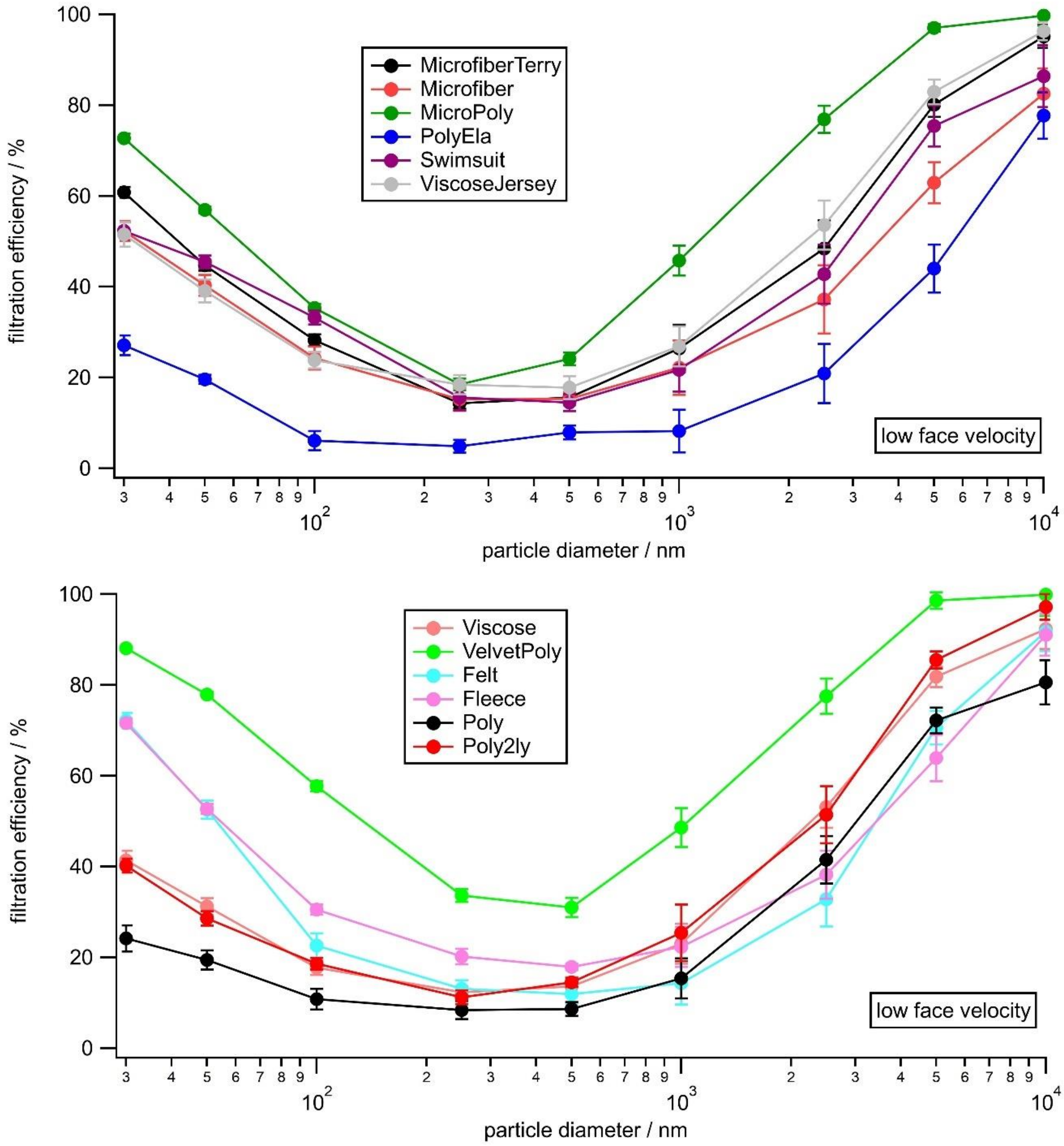

Figure S3a: Size-dependent filtration efficiency (ambient aerosol, measured with the *SMPS/OPC setup*, low face velocity) for “synthetic fiber” materials.

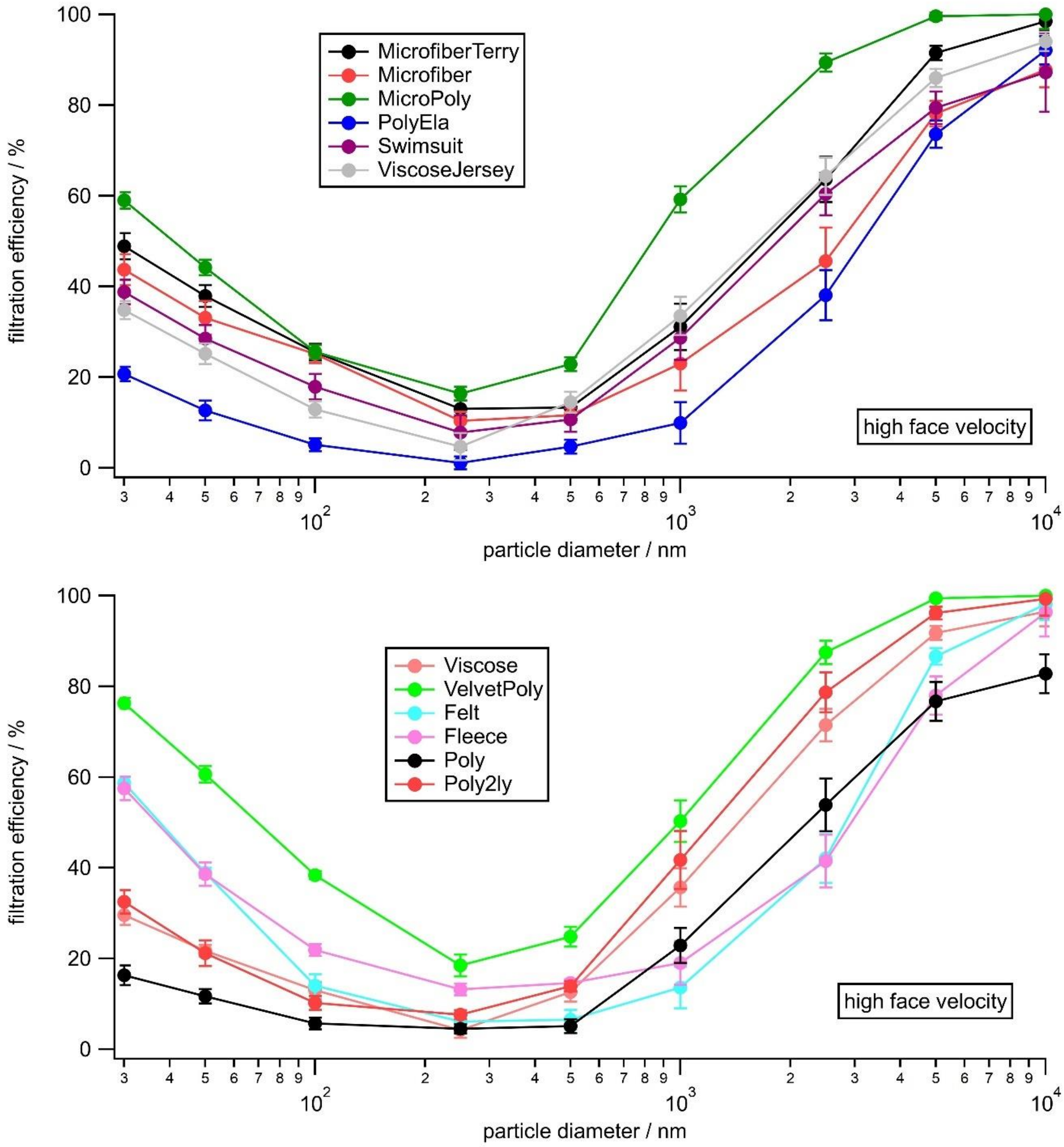

Figure S3b: Size-dependent filtration efficiency (ambient aerosol, measured with the *SMPS/OPC setup*, high face velocity) for “synthetic fiber” materials.

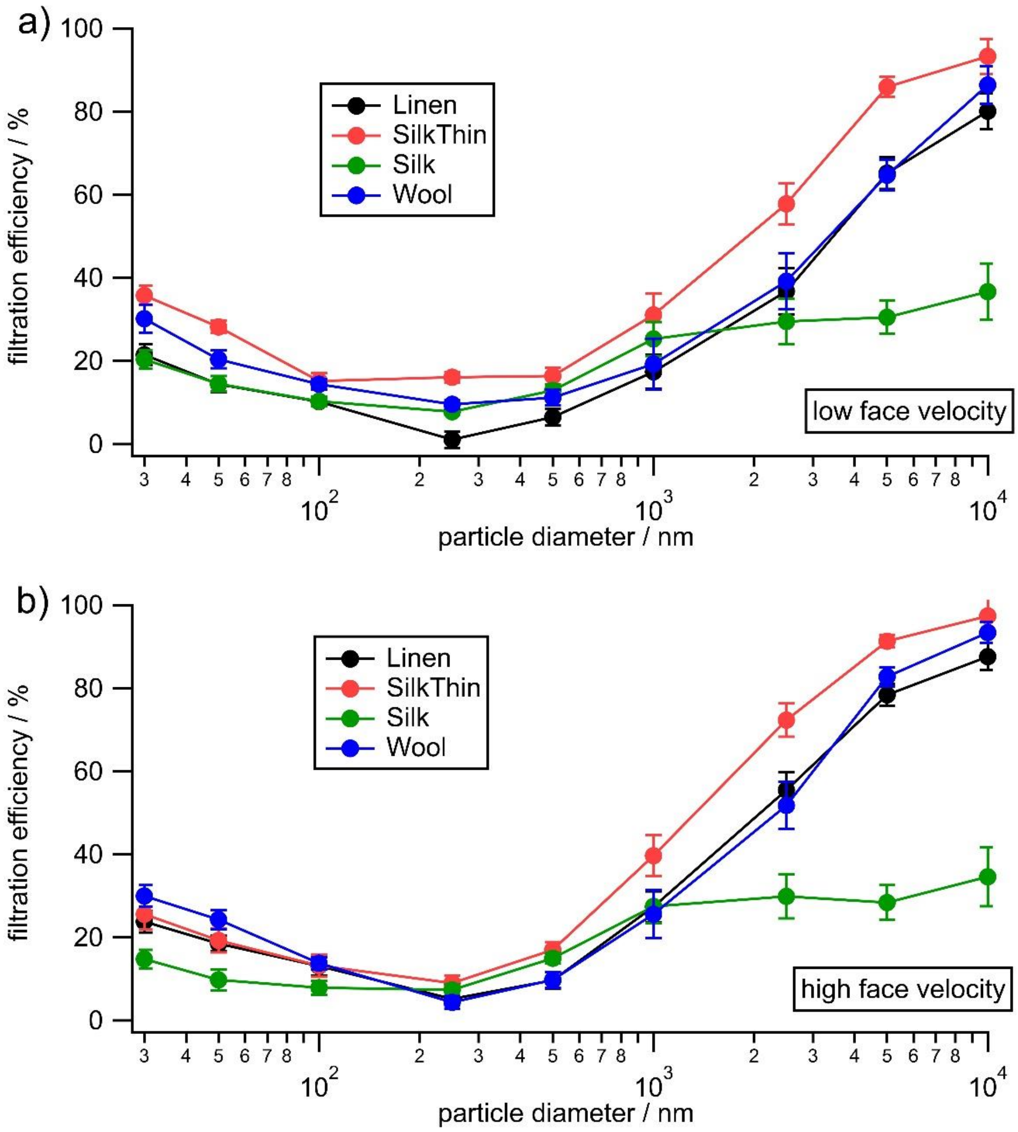

Figure S4: Size-dependent filtration efficiency (ambient aerosol, measured with the *SMPS/OPC setup*) for “natural fiber” materials, for a) low and b) high face velocity.

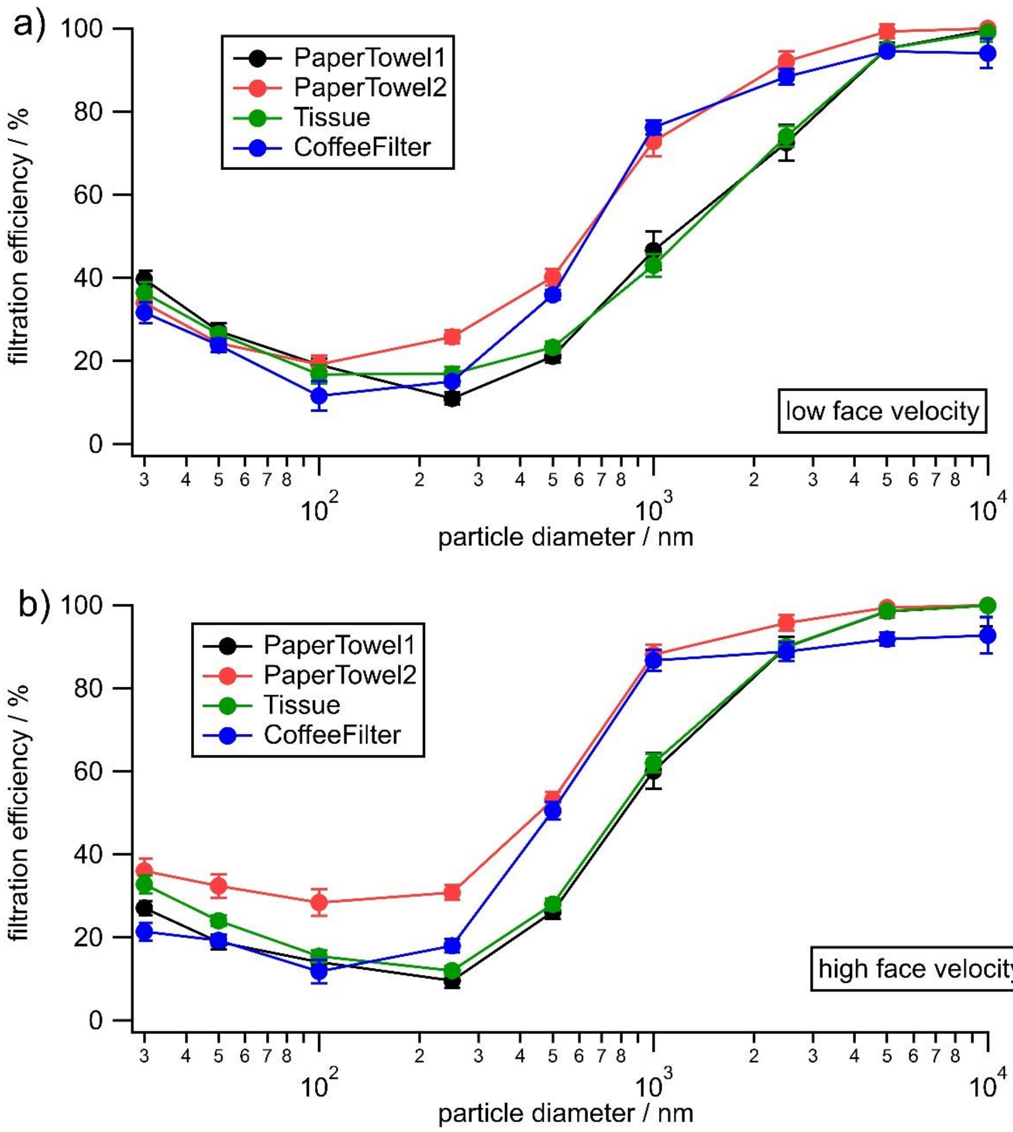

Figure S5: Size-dependent filtration efficiency (ambient aerosol, measured with the *SMPS/OPC setup*) for "paper-like" materials, measured at a) low and b) high face velocity.

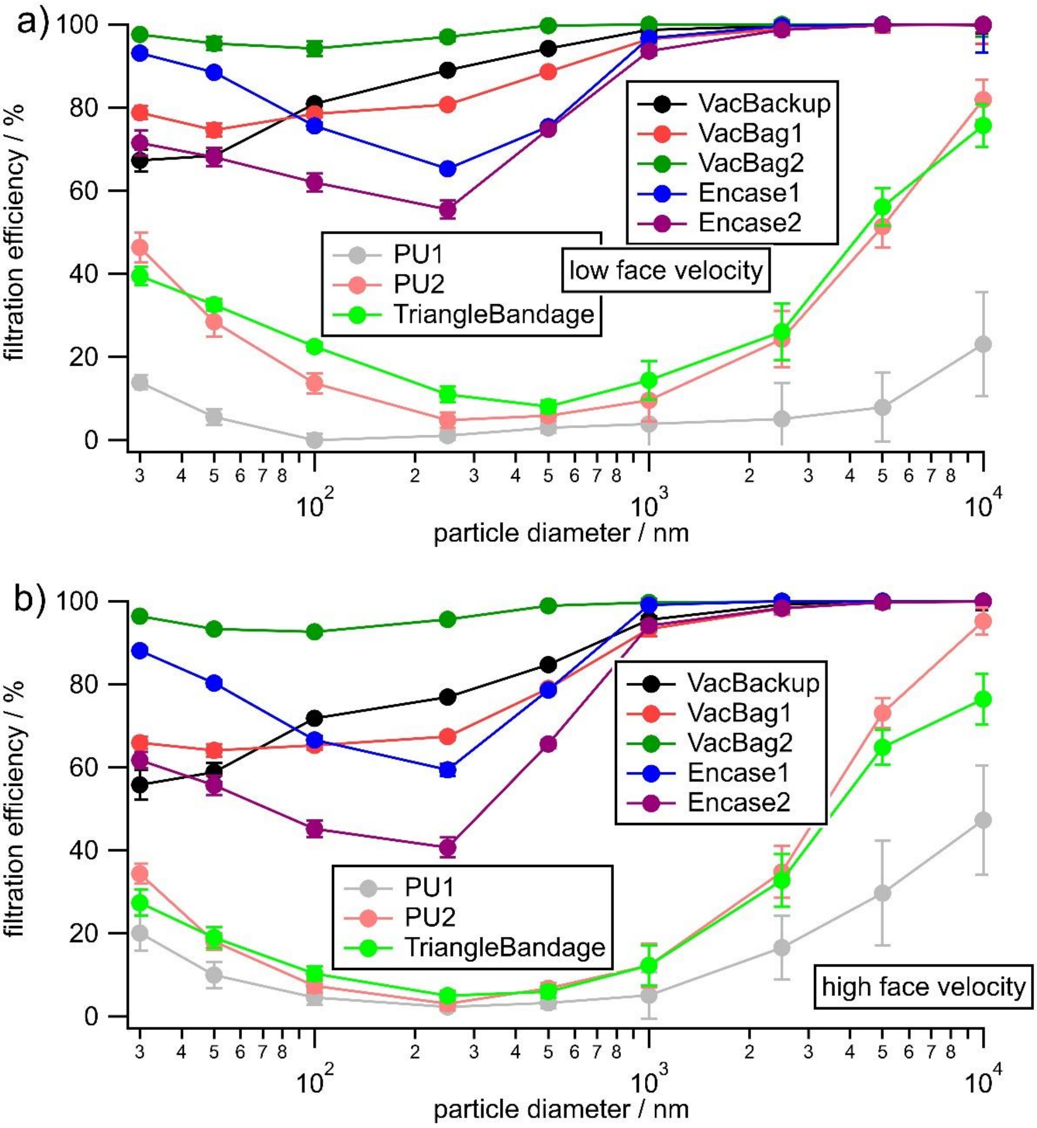

Figure S6: Size-dependent filtration efficiency (ambient aerosol, measured with the *SMPS/OPC setup*) for “other synthetic household materials”, measured at a) low and b) high face velocity.

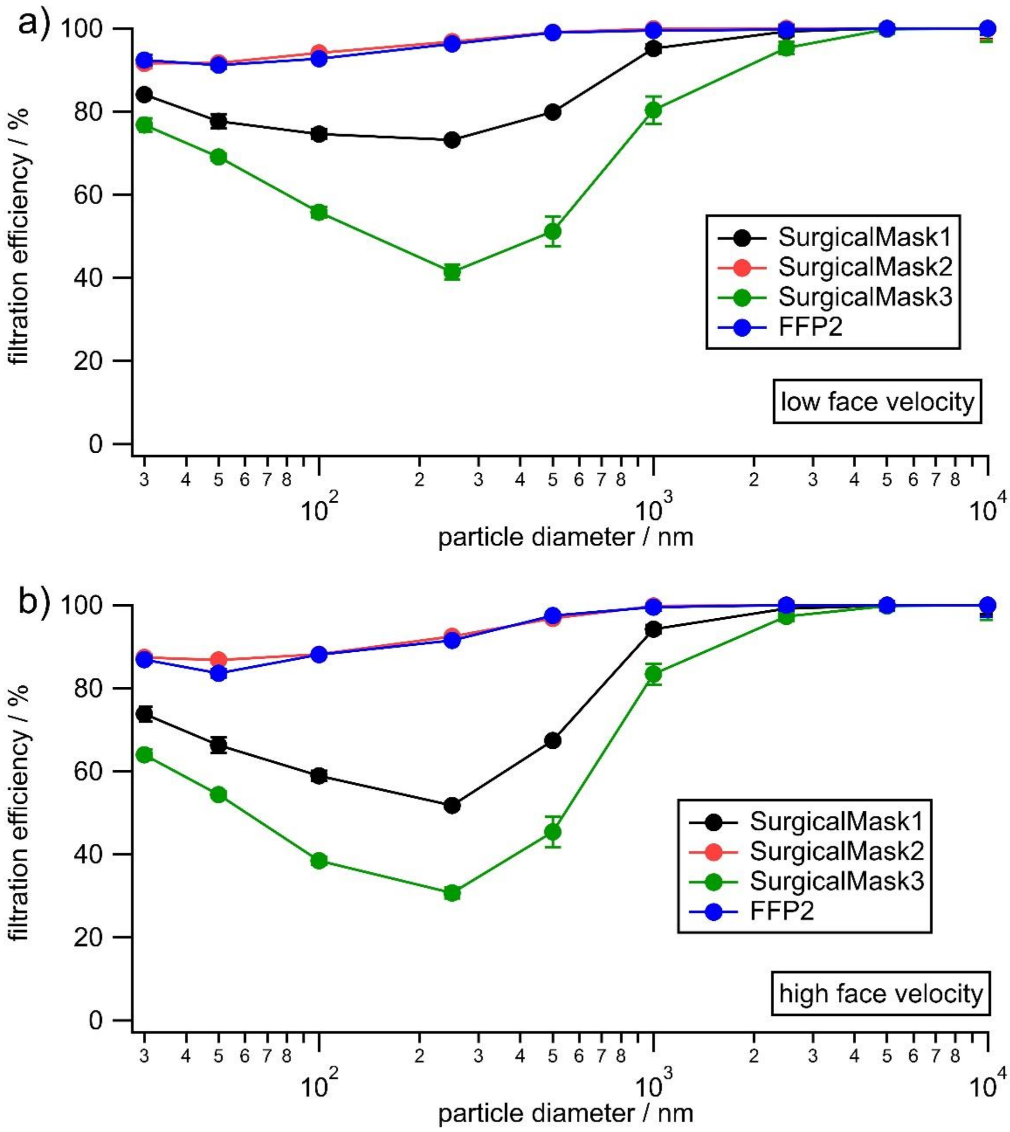

Figure S7: Size-dependent filtration efficiency (ambient aerosol, measured with the *SMPS/OPC setup*) for “medical masks”, measured at a) low and b) high face velocity.

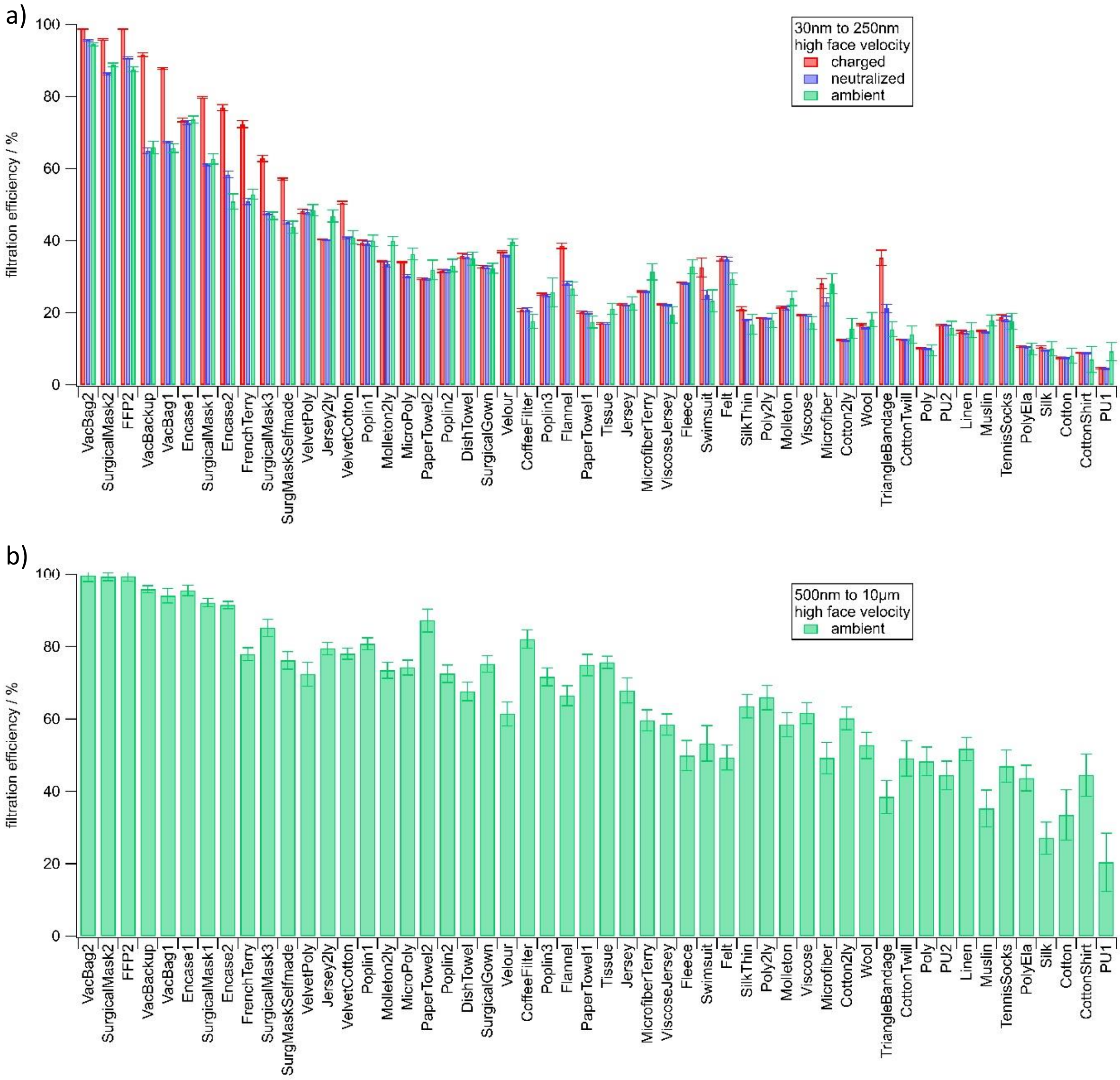

Figure S8: Average filtration efficiencies for a) small (d_p=30 nm to 250 nm, measured with the *CPC setup* and the *SMPS/OPC setup*) and b) large (d_p=500 nm to 10 µm, measured with the *SMPS/OPC setup*) particles, measured at high face velocity. Materials are sorted as in Fig. 3 in the main text.

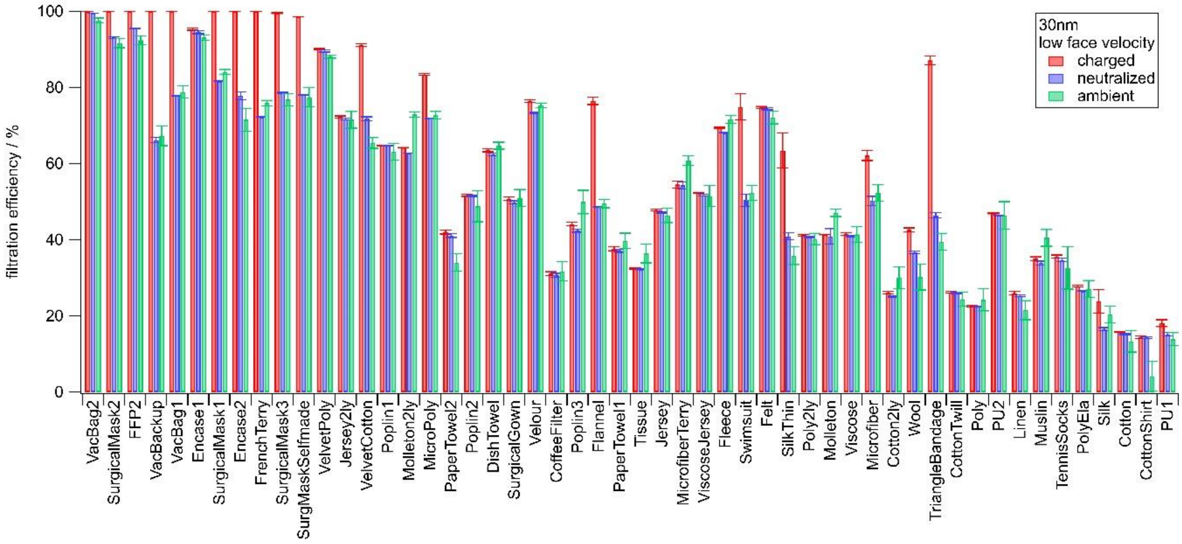

Figure S9: Filtration efficiencies for d_p=30 nm particles, measured at low face velocity with the *CPC setup* and the *SMPS/OPC setup*. Materials are sorted as in Fig. 3 in the main text.

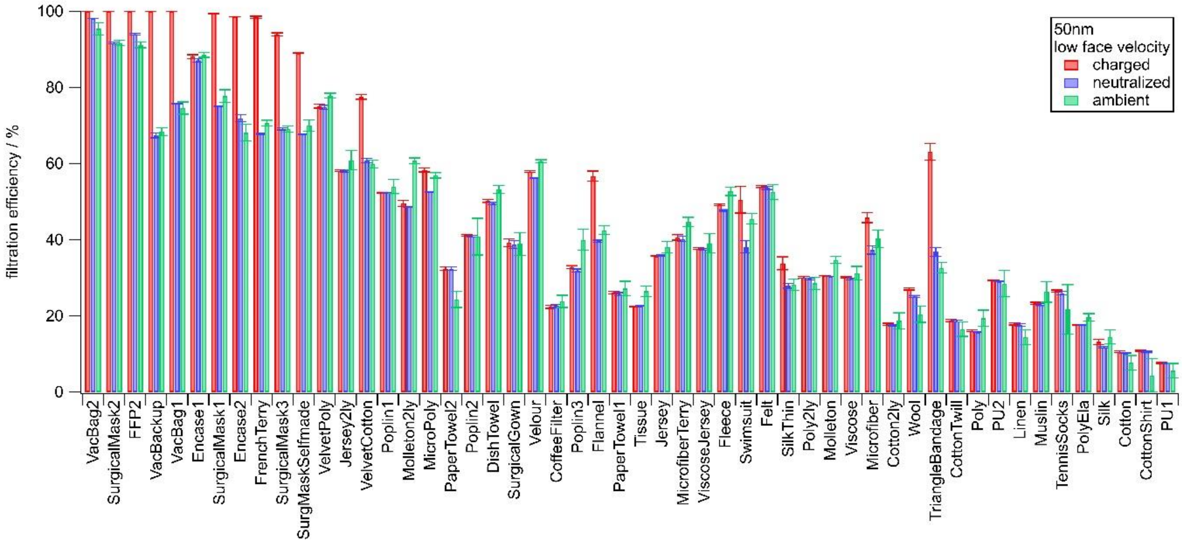

Figure S10: Filtration efficiencies for d_p=50 nm particles, measured at low face velocity with the *CPC setup* and the *SMPS/OPC setup*. Materials are sorted as in Fig. 3 in the main text.

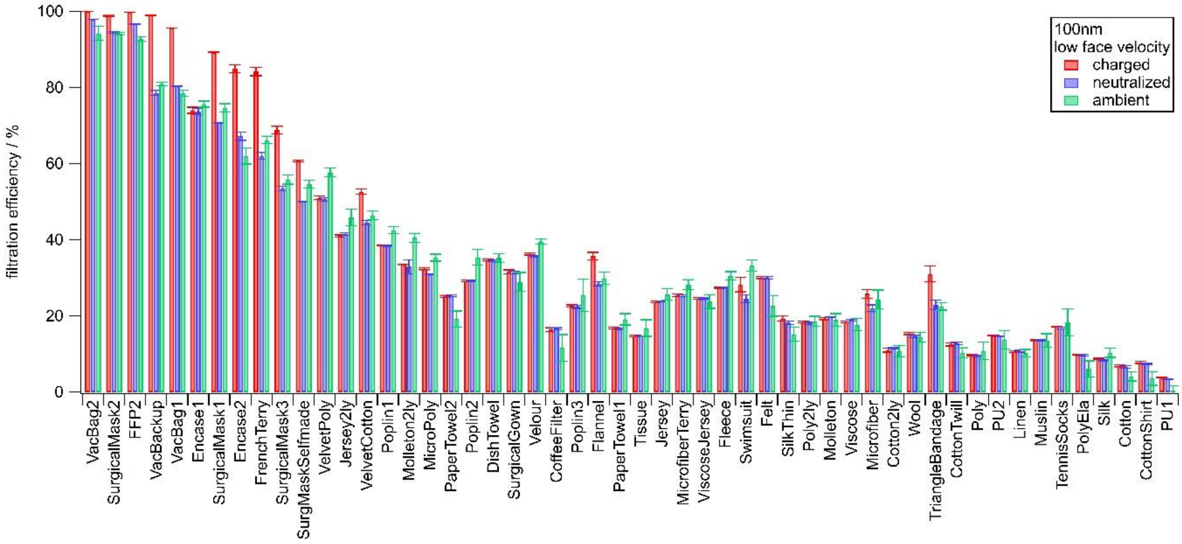

Figure S11: Filtration efficiencies for d_p=100 nm particles, measured at low face velocity with the *CPC setup* and the *SMPS/OPC setup*. Materials are sorted as in Fig. 3 in the main text.

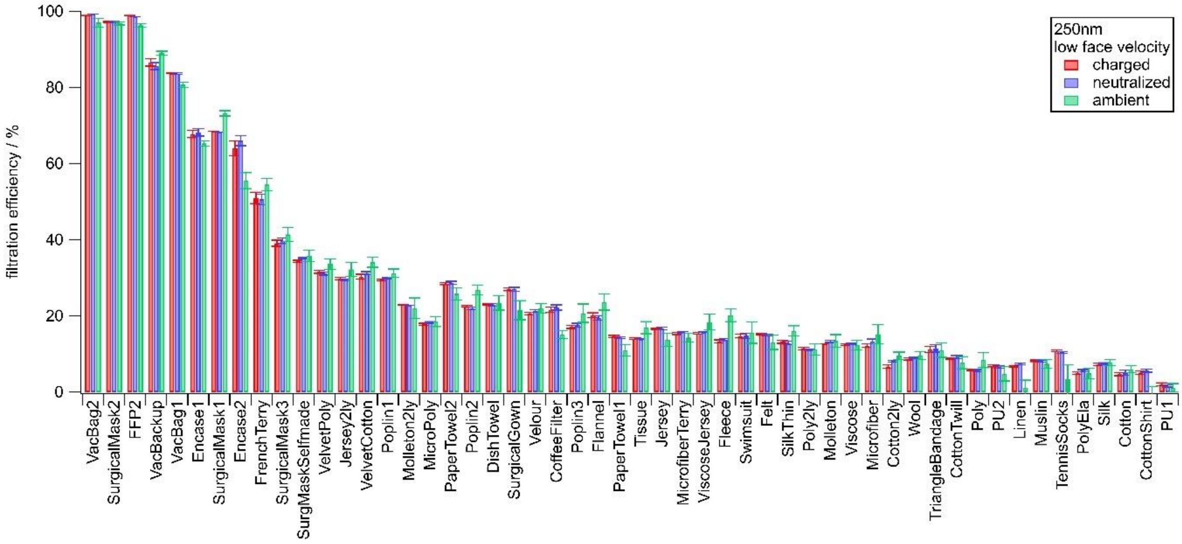

Figure S12: Filtration efficiencies for d_p=250 nm particles, measured at low face velocity with the *CPC setup* and the *SMPS/OPC setup*. Materials are sorted as in Fig. 3 in the main text.

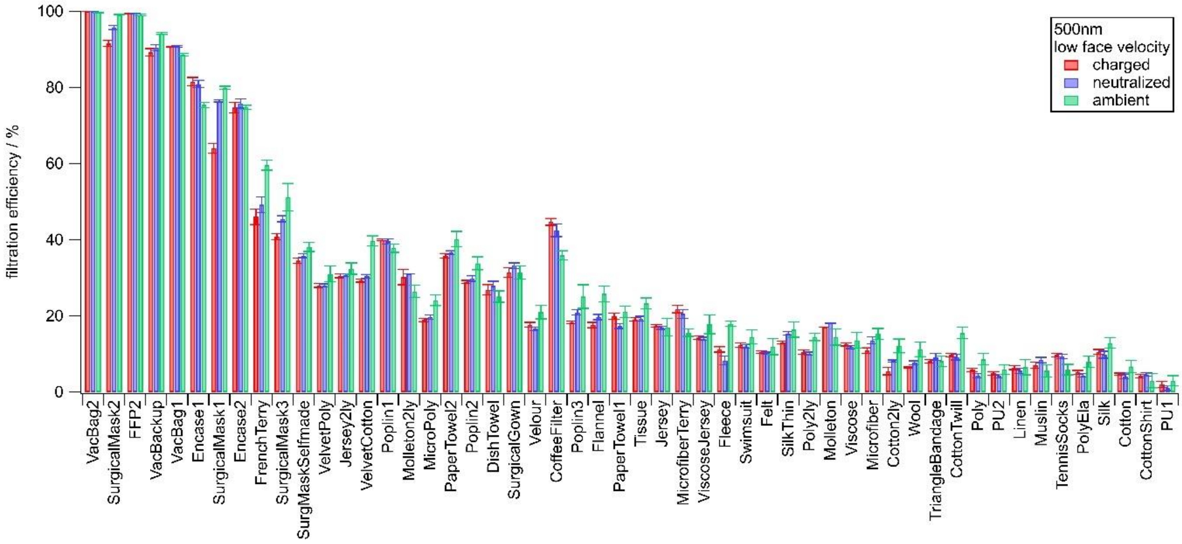

Figure S13: Filtration efficiencies for d_p=500 nm particles, measured at low face velocity with the *CPC setup* and the *SMPS/OPC setup*. Materials are sorted as in Fig. 3 in the main text.

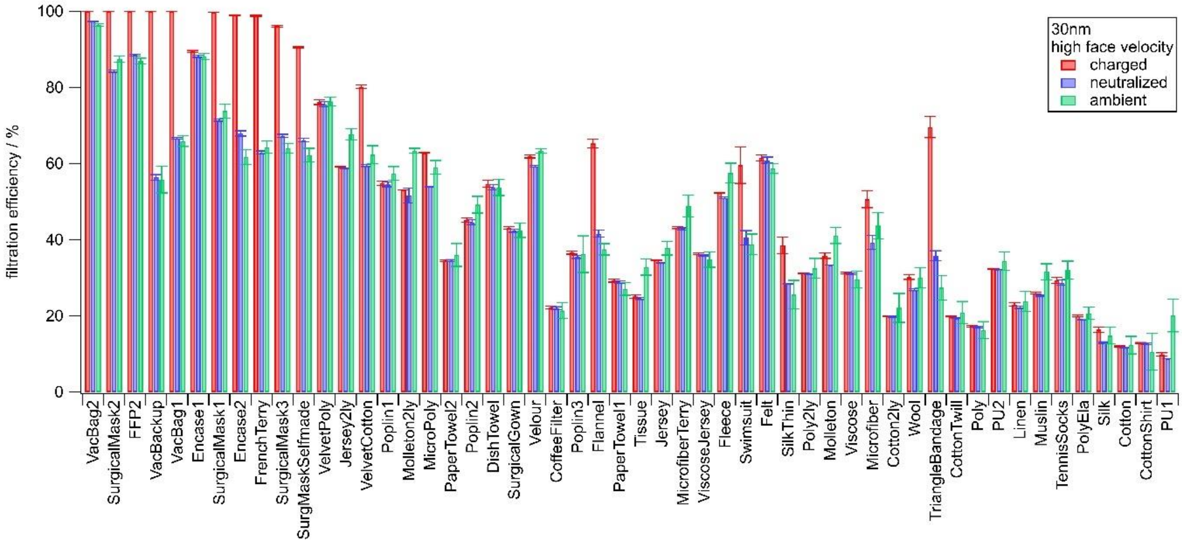

Figure S14: Filtration efficiencies for d_p=30 nm particles, measured at high face velocity with the *CPC setup* and the *SMPS/OPC setup*. Materials are sorted as in Fig. 3 in the main text.

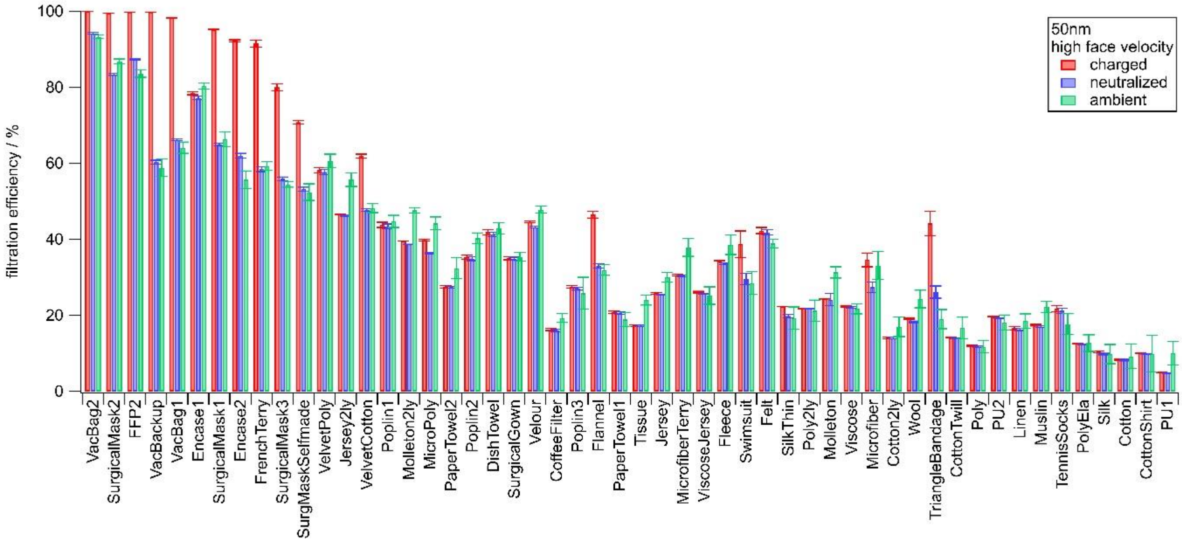

Figure S15: Filtration efficiencies for d_p=50 nm particles, measured at high face velocity with the *CPC setup* and the *SMPS/OPC setup*. Materials are sorted as in Fig. 3 in the main text.

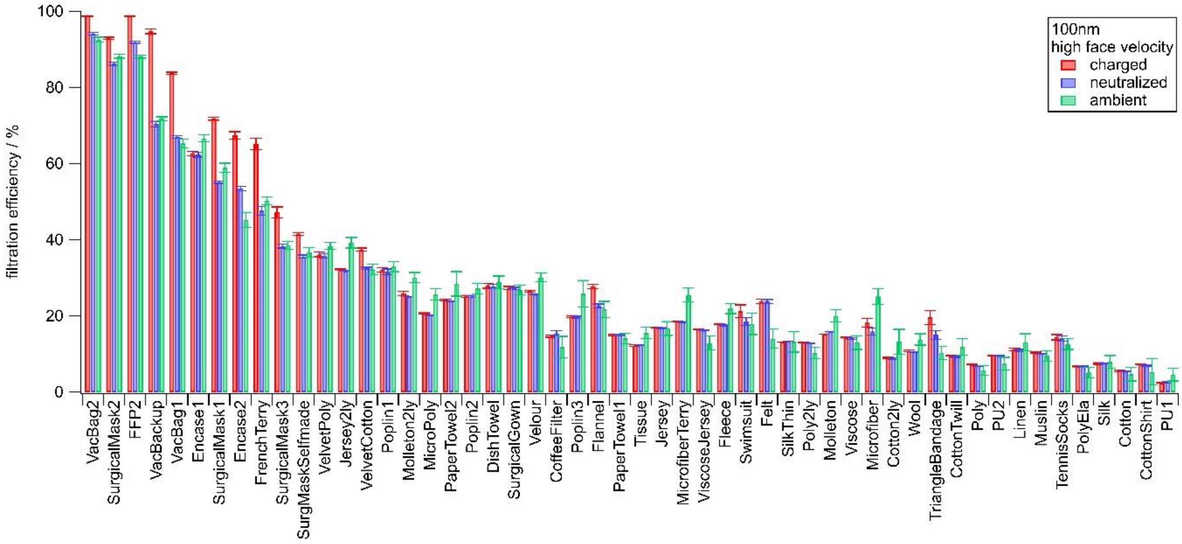

Figure S16: Filtration efficiencies for d_p=100 nm particles, measured at high face velocity with the *CPC setup* and the *SMPS/OPC setup*. Materials are sorted as in Fig. 3 in the main text.

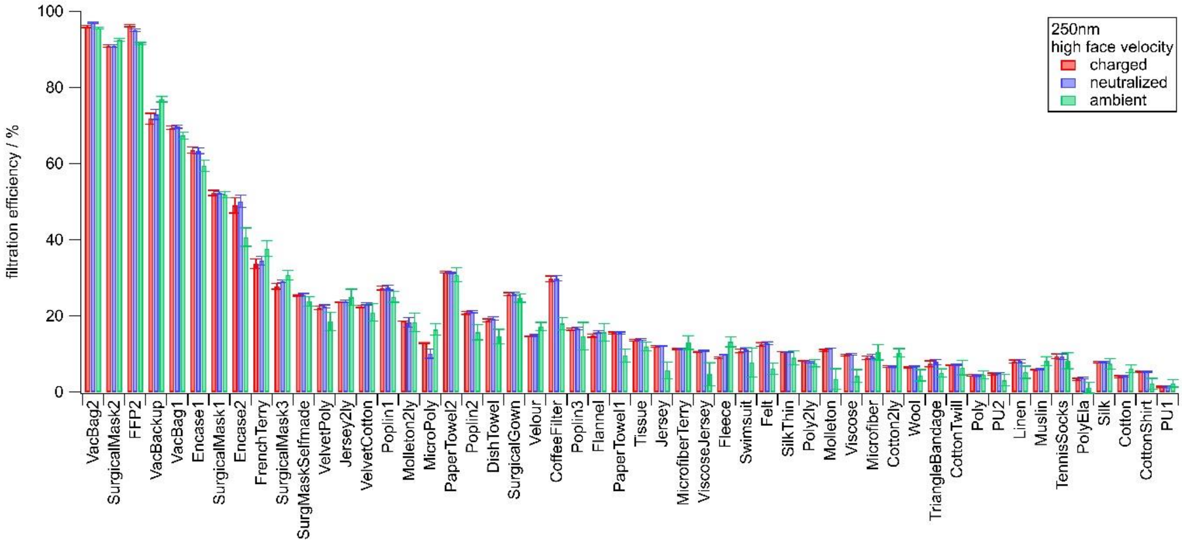

Figure S17: Filtration efficiencies for d_p=250 nm particles, measured at high face velocity with the *CPC setup* and the *SMPS/OPC setup*. Materials are sorted as in Fig. 3 in the main text.

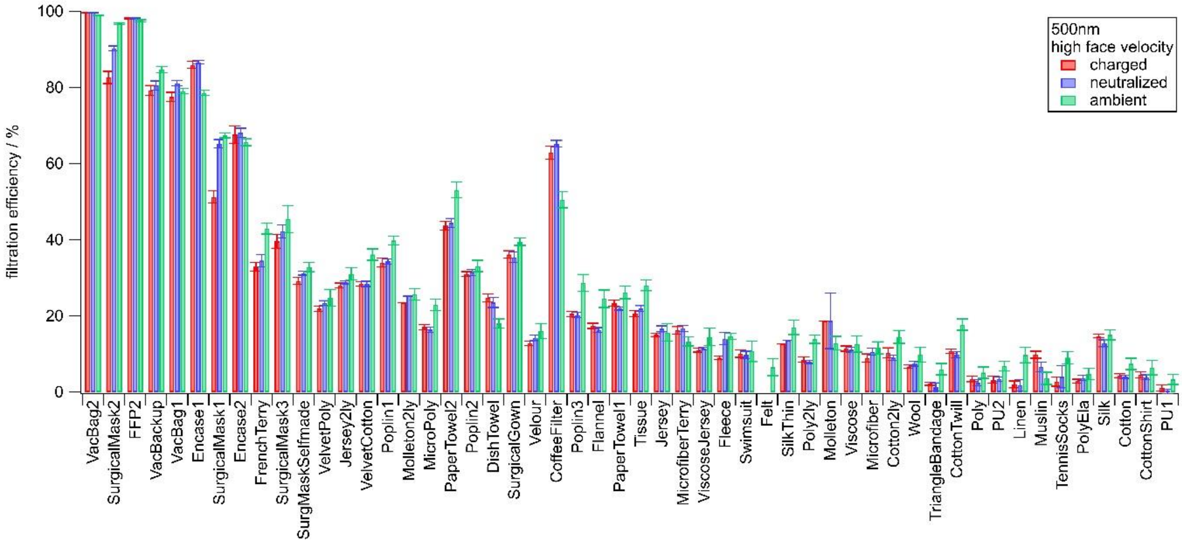

Figure S18: Filtration efficiencies for d_p=500 nm particles, measured at high face velocity with the *CPC setup* and the *SMPS/OPC setup*. Materials are sorted as in Fig. 3 in the main text.

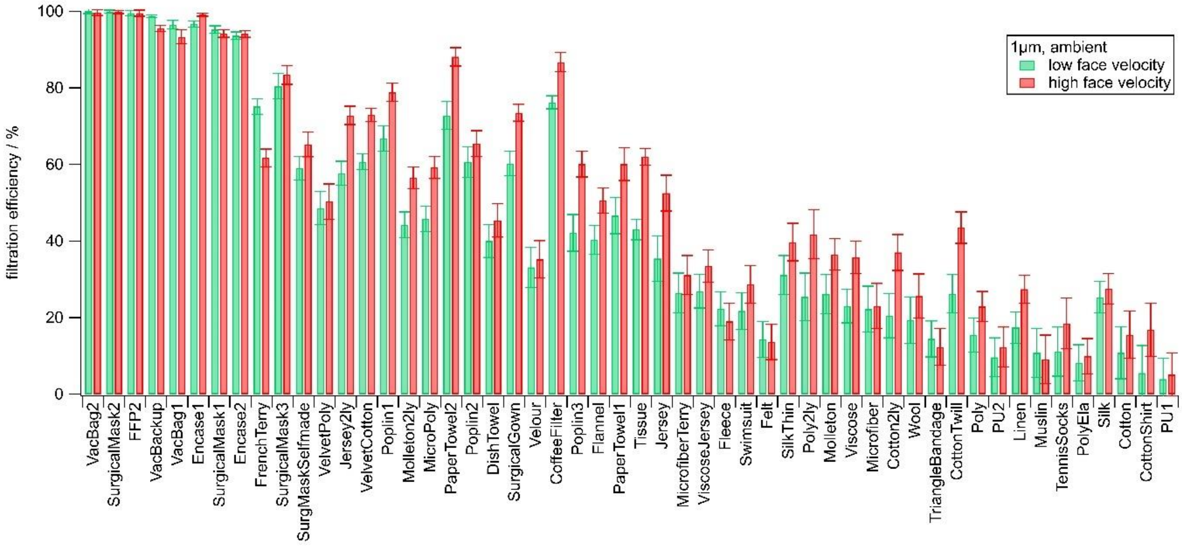

Figure S19: Filtration efficiencies for d_p=1 µm particles, measured at low and high face velocity with the *SMPS/OPC setup*. Materials are sorted as in Fig. 3 in the main text.

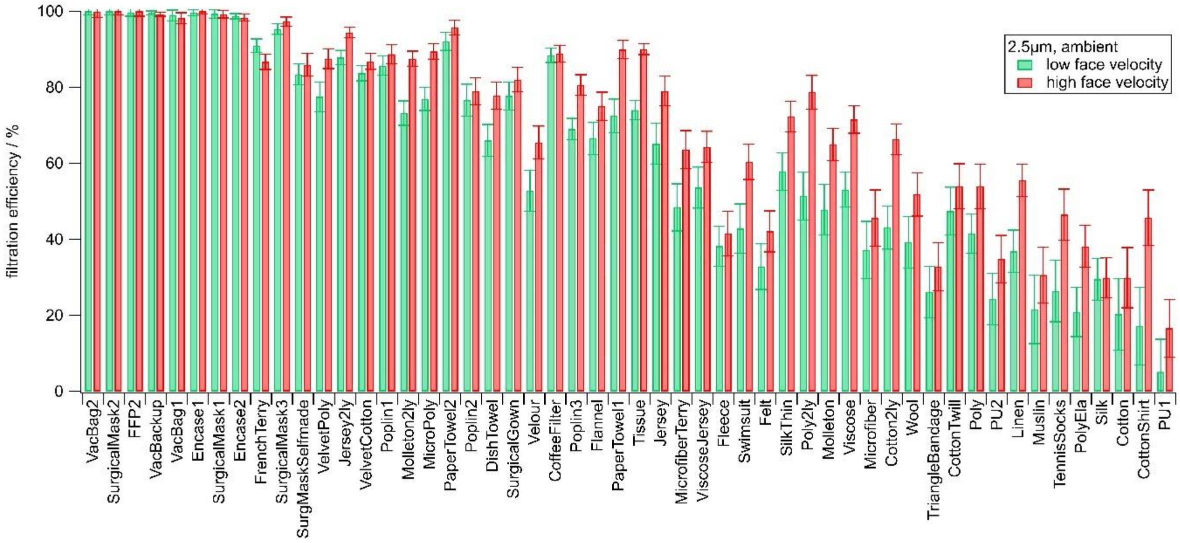

Figure S20: Filtration efficiencies for d_p=2.5 µm particles, measured at low and high face velocity with the *SMPS/OPC setup*. Materials are sorted as in Fig. 3 in the main text.

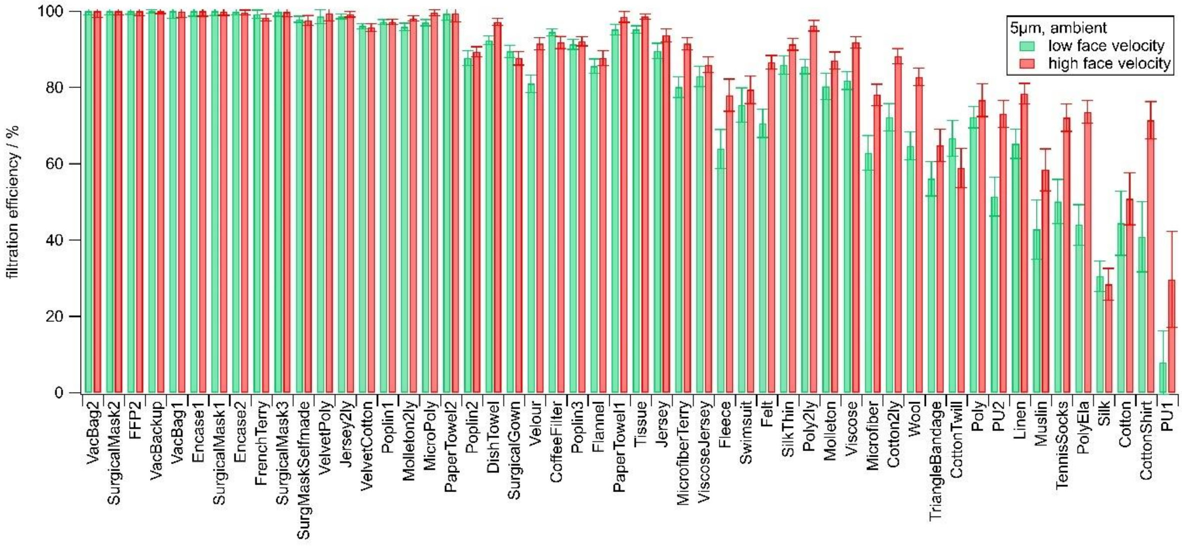

Figure S21: Filtration efficiencies for d_p=5 µm particles, measured at low and high face velocity with the *SMPS/OPC setup*. Materials are sorted as in Fig. 3 in the main text.

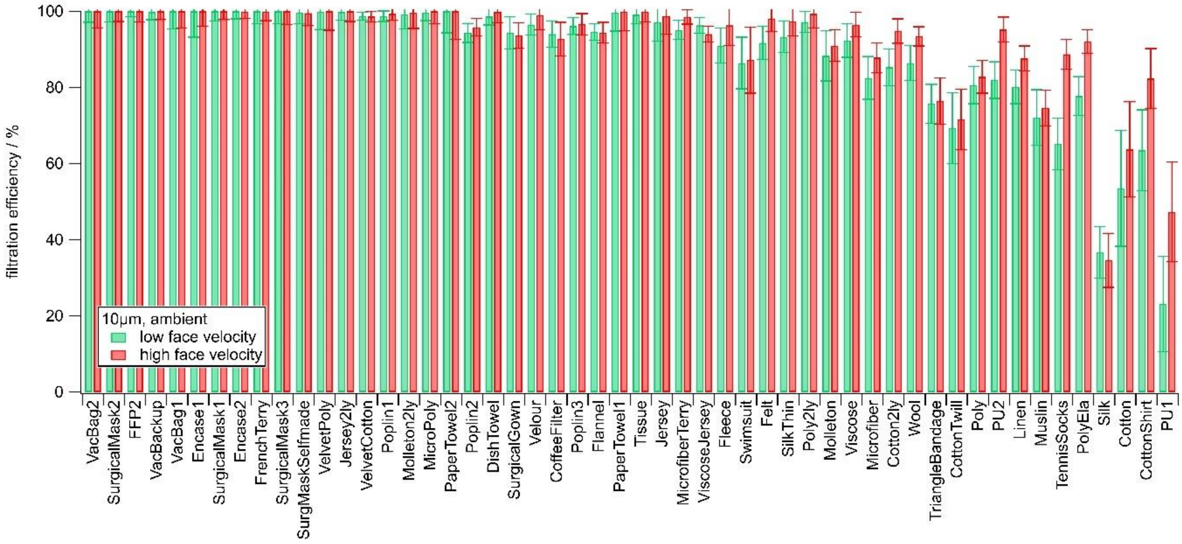

Figure S22: Filtration efficiencies for d_p=10 µm particles, measured at low and high face velocity with the *SMPS/OPC setup*. Materials are sorted as in Fig. 3 in the main text.

Table S2: Fitting coefficients for fits according to $\Delta p(v_f) = \Delta p(0) + A_{\Delta p}\, v_f^s$ in Fig. 4a with v_f in units of cm s^{-1}. The uncertainties are one standard deviation of the fitting coefficients, provided by the fitting algorithm.

Material	**$\Delta p(0)$ / Pa**	**$A_{\Delta p}$ / Pa**	***s***
Jersey2ly	-2.8 ± 1.0	35.1 ± 0.7	0.80 ± 0.01
Molleton2ly	1.8 ± 0.9	5.7 ± 0.3	1.10 ± 0.01
Cotton2ly	2.0 ± 0.8	2.9 ± 0.2	1.22 ± 0.02
Poly2ly	1.9 ± 0.9	5.5 ± 0.3	1.12 ± 0.01

Table S3: Fitting coefficients for fits according to $FE(v_f)= FE_{asympt} + A_{FE} \exp(-v_f\, \tau^{-1})$ in Fig. 4b for the particle sizes 30 to 250 nm from measurements of neutralized aerosol (*CPC setup*), with v_f in units of cm s^{-1}. The uncertainties are one standard deviation of the fitting coefficients, provided by the fitting algorithm.

Material	**Particle diameter / nm**	**FE_{asympt} / %**	**A_{FE} / %**	**τ / cm s^{-1}**
Jersey2ly	30	47.9 ± 0.9	44.2 ± 0.6	9.1 ± 0.5
	50	38.9 ± 0.8	41.4 ± 0.3	7.3 ± 0.4
	100	26.3 ± 0.6	35.9 ± 0.3	6.8 ± 0.4
	250	22.3 ± 0.5	26.2 ± 0.9	4.3 ± 0.3
Molleton2ly	30	43.5 ± 0.9	41.9 ± 0.8	8.7 ± 0.6
	50	32.3 ± 0.6	39.1 ± 0.7	7.9 ± 0.5
	100	21.3 ± 0.3	31.2 ± 0.5	6.9 ± 0.3
	250	17.5 ± 0.3	18.8 ± 0.7	5.4 ± 0.5
Cotton2ly	30	18.4 ± 0.2	24.1 ± 0.6	4.7 ± 0.2
	50	13.1 ± 0.2	15.6 ± 0.5	5.6 ± 0.3
	100	8.8 ± 0.2	11.3 ± 1.5	4.0 ± 0.6
	250	6.9 ± 0.2	8.9 ± 2.2	2.7 ± 0.6
Poly2ly	30	26.1 ± 0.3	34.5 ± 0.2	6.7 ± 0.2
	50	18.4 ± 0.3	28.7 ± 0.5	6.0 ± 0.3
	100	11.1 ± 0.2	20.0 ± 0.5	5.5 ± 0.3
	250	7.8 ± 0.2	12.7 ± 1.0	4.0 ± 0.4

Table S4: Fitting coefficients for fits according to $FE(v_f) = FE_{asympt} + A_{FE}\exp(-v_f\,\tau^{-1})$ in Fig. 4d for the particle sizes 2500 to 10000 nm from measurements of ambient aerosol (*SMPS/OPC setup*), with v_f in units of cm s^{-1}. Some fits gave unreasonable results because measured *FE* was close to 100% for all face velocities. These are shown in italics. The uncertainties are one standard deviation of the fitting coefficients, provided by the fitting algorithm.

Material	**Particle diameter / nm**	FE_{asympt} **/ %**	A_{FE} **/ %**	**τ / cm s^{-1}**
Jersey2ly	2500	97.0 ± 1.5	-16.8 ± 5.4	5.6 ± 2.7
	5000	*98.9 ± 5.2e+05*	*0.1 ± 5.2e+05*	*6187.6 ± 2.7e+10*
	10000	*-269.71 ± 1.1e+07*	*369.79 ± 1.1e+07*	*16719 ± 5.2e+08*
Molleton2ly	2500	89.6 ± 3. 5	-43.6 ± 15.5	5.3 ± 2.6
	5000	97.5 ± 0.7	-12.3 ± 15.7	2.7 ± 2.4
	10000	*99.3 ± 2.0*	*-58.9 ± 11889*	*0.7 ± 33.3*
Cotton2ly	2500	88.2 ± 8.3	-70.9 ± 8.6	11.0 ± 4.6
	5000	92.7 ± 2.0	-44.5 ± 9.4	6.1 ± 1.8
	10000	97.9 ± 9.2	-15.5 ± 7.7	11.0 ± 18.6
Poly2ly	2500	93.0 ± 6.2	-67.5 ± 11.0	8.5 ± 3.4
	5000	99.1 ± 3.2	-36.5 ± 8.7	5.2 ± 2.4
	10000	100.0 ± 8. 5	-7.3 ± 10.3	5.4 ± 23.5

Table S5: Fitting coefficients according to $\Delta p(n) = \Delta p(0) + slope_P \cdot n$ (with number of layers n and $\Delta p(n)$ the corresponding pressure drop in Pa) in Fig. 5a in the main text. The uncertainties are one standard deviation of the fitting coefficients, provided by the fitting algorithm.

Material	**Face velocity**	$\Delta p(0)$ **/ Pa**	$slope_P$ **/ Pa**
Jersey	Low	-10.18 ± 2.83	69.20 ± 1.38
	High	-18.84 ± 3.38	146.04 ± 1.75
Molleton	Low	-0.30 ± 1.32	20.19 ± 0.41
	High	-0.86 ± 1.31	48.79 ± 0.54
Cotton	Low	0.65 ± 1.07	13.20 ± 0.32
	High	-1.90 ± 1.05	34.30 ± 0.33
Polyester	Low	4.65 ± 1.07	17.20 ± 0.32
	High	7.40 ± 1.20	43.19 ± 0.46

Table S6: Measured transmission efficiencies (ambient aerosol, *SMPS/OPC setup*) for 1 layer ($T(1)_{measured}$), and fit coefficients $T(1)_{fit}$ for fits according to $T(n)=T(1)^n$ (with n the number of layers) in Fig. 5b. The uncertainties are one standard deviation of the fitting coefficients, provided by the fitting algorithm.

Material	**Particle diameter / nm**	**Low face velocity**		**High face velocity**	
		$\mathbf{T(1)_{measured}}$	$\mathbf{T(1)_{fit}}$	$\mathbf{T(1)_{measured}}$	$\mathbf{T(1)_{fit}}$
Jersey	30	0.54 ± 0.019	0.52 ± 0.004	0.62 ± 0.018	0.58 ± 0.004
	50	0.62 ± 0.015	0.60 ± 0.004	0.70 ± 0.013	0.65 ± 0.003
	100	0.74 ± 0.015	0.71 ± 0.003	0.83 ± 0.018	0.76 ± 0.003
	250	0.86 ± 0.017	0.81 ± 0.002	0.94 ± 0.022	0.85 ± 0.003
	500	0.83 ± 0.023	0.81 ± 0.003	0.84 ± 0.023	0.82 ± 0.003
	1000	0.65 ± 0.059	0.64 ± 0.010	0.48 ± 0.047	0.53 ± 0.011
	2500	0.35 ± 0.054	0.35 ± 0.019	0.21 ± 0.039	0.23 ± 0.022
	5000	0.10 ± 0.02	0.11 ± 0.016	0.06 ± 0.017	0.07 ± 0.016
	10000	0.03 ± 0.049	0.03 ± 0.049	0.01 ± 0.048	0.01 ± 0.048
Molleton	30	0.53 ± 0.01	0.54 ± 0.004	0.59 ± 0.021	0.62 ± 0.003
	50	0.65 ± 0.009	0.65 ± 0.003	0.69 ± 0.015	0.72 ± 0.003
	100	0.81 ± 0.017	0.77 ± 0.003	0.80 ± 0.016	0.82 ± 0.002
	250	0.87 ± 0.017	0.86 ± 0.004	0.97 ± 0.027	0.89 ± 0.004
	500	0.86 ± 0.021	0.86 ± 0.003	0.87 ± 0.018	0.87 ± 0.003
	1000	0.74 ± 0.051	0.75 ± 0.012	0.64 ± 0.041	0.67 ± 0.013
	2500	0.52 ± 0.067	0.54 ± 0.020	0.35 ± 0.043	0.37 ± 0.021
	5000	0.20 ± 0.035	0.20 ± 0.020	0.13 ± 0.022	0.13 ± 0.017
	10000	0.12 ± 0.066	0.11 ± 0.061	0.09 ± 0.042	0.09 ± 0.041
Cotton	30	0.87 ± 0.028	0.85 ± 0.005	0.88 ± 0.023	0.89 ± 0.005
	50	0.92 ± 0.019	0.90 ± 0.003	0.91 ± 0.032	0.93 ± 0.004
	100	0.96 ± 0.012	0.95 ± 0.002	0.95 ± 0.018	0.95 ± 0.002
	250	0.94 ± 0.009	0.96 ± 0.002	0.94 ± 0.010	0.96 ± 0.002
	500	0.93 ± 0.016	0.95 ± 0.002	0.93 ± 0.015	0.94 ± 0.002
	1000	0.89 ± 0.068	0.90 ± 0.008	0.85 ± 0.062	0.80 ± 0.008
	2500	0.80 ± 0.094	0.75 ± 0.012	0.70 ± 0.079	0.58 ± 0.013
	5000	0.56 ± 0.084	0.50 ± 0.016	0.49 ± 0.068	0.35 ± 0.019
	10000	0.47 ± 0.152	0.38 ± 0.049	0.36 ± 0.125	0.25 ± 0.054
Polyester	30	0.76 ± 0.029	0.75 ± 0.003	0.84 ± 0.022	0.82 ± 0.003
	50	0.81 ± 0.021	0.82 ± 0.003	0.88 ± 0.016	0.87 ± 0.002
	100	0.89 ± 0.023	0.90 ± 0.003	0.94 ± 0.013	0.93 ± 0.003
	250	0.92 ± 0.020	0.94 ± 0.002	0.96 ± 0.010	0.96 ± 0.002
	500	0.91 ± 0.015	0.93 ± 0.002	0.95 ± 0.015	0.94 ± 0.002
	1000	0.85 ± 0.044	0.86 ± 0.011	0.77 ± 0.039	0.78 ± 0.011
	2500	0.59 ± 0.052	0.67 ± 0.016	0.46 ± 0.058	0.46 ± 0.021
	5000	0.28 ± 0.028	0.35 ± 0.018	0.23 ± 0.043	0.21 ± 0.026
	10000	0.19 ± 0.049	0.19 ± 0.041	0.17 ± 0.043	0.16 ± 0.040

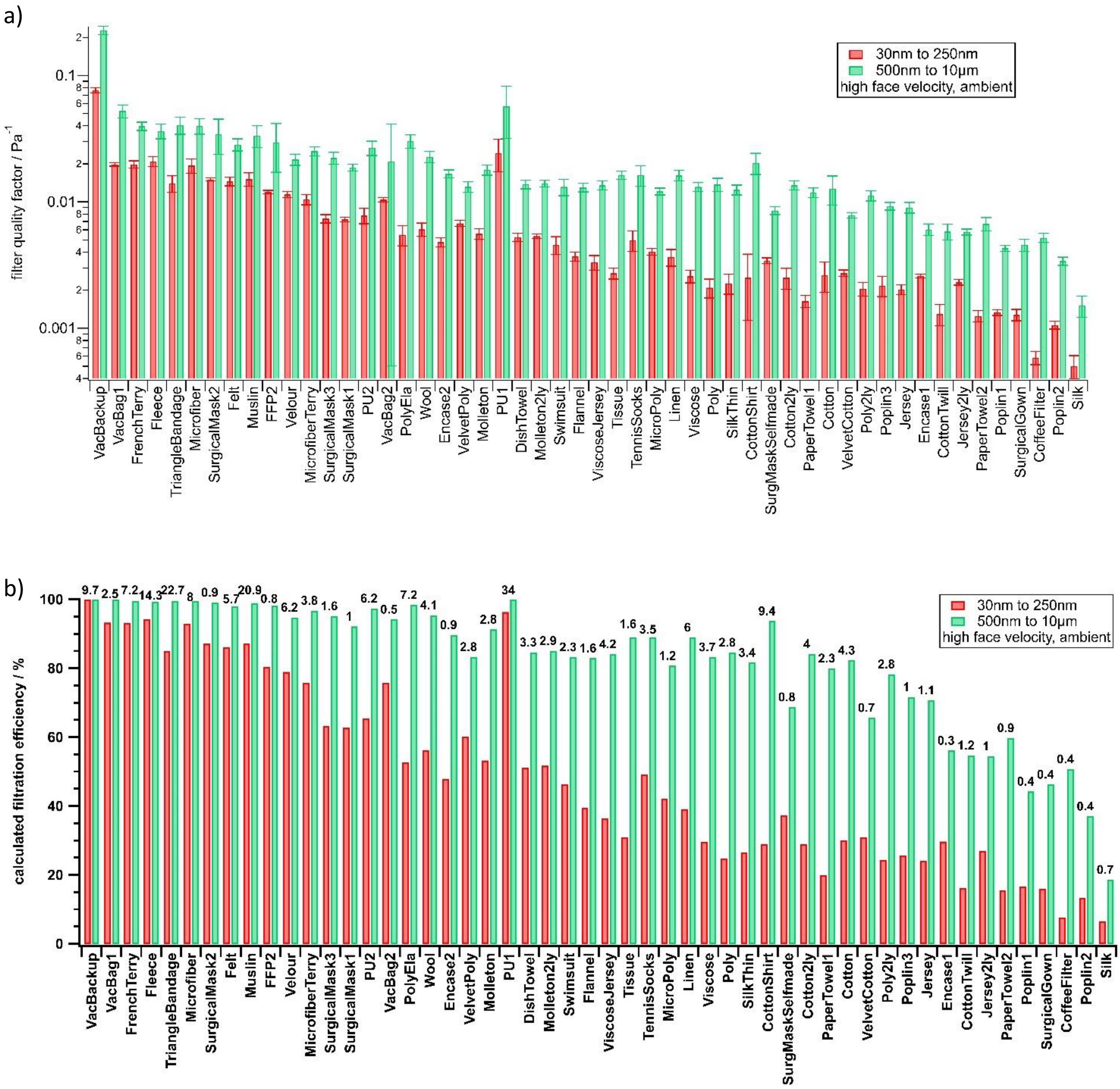

Figure S23: a) Filter quality factor and b) calculated filtration efficiency for small and large particles, ambient aerosol (*SMPS/OPC setup*), at high face velocity. Materials are sorted as in Fig. 6 in the main text.

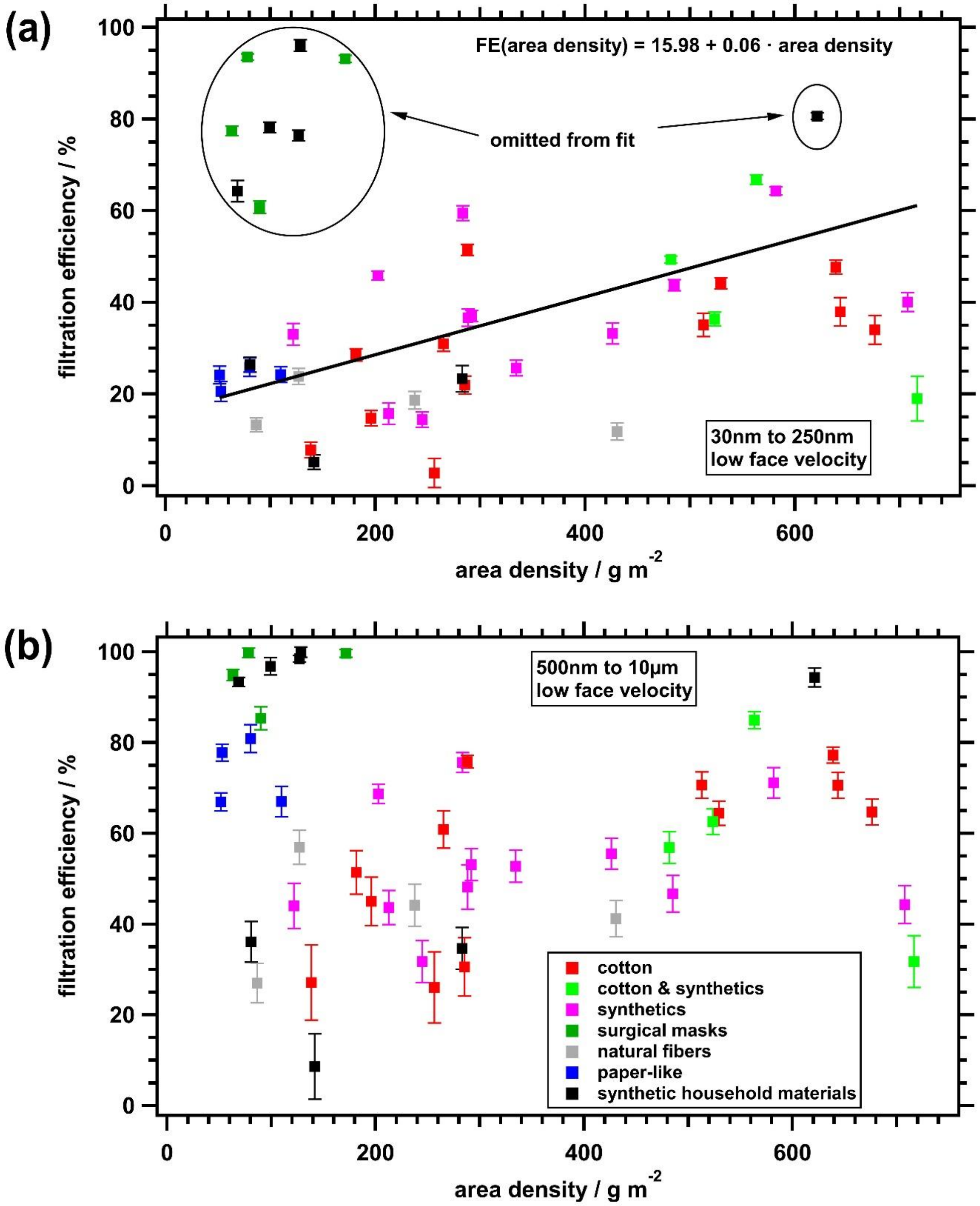

Figure S24: Dependence of filtration efficiency on area density (in g m^{-2}) for a) small (d_p=30 nm to 250 nm) and b) large particles (d_p=500 nm to 10 µm), for ambient aerosol (*SMPS/OPC setup*) at low face velocity.

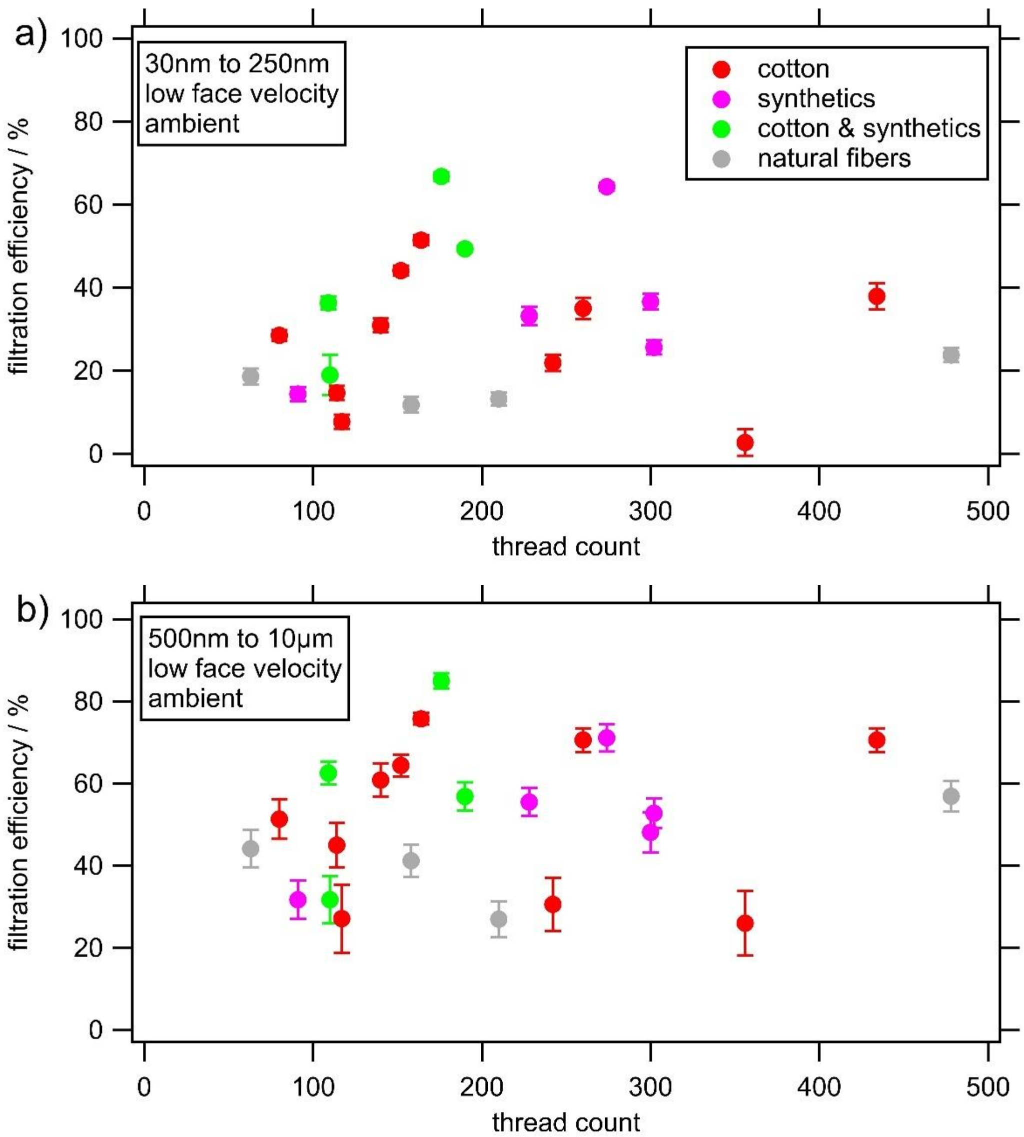

Figure S25: Filtration efficiency versus thread count for a) small and b) large particles, color-coded for material type. Ambient aerosol, measured with the *SMPS/OPC setup*, low face velocity.

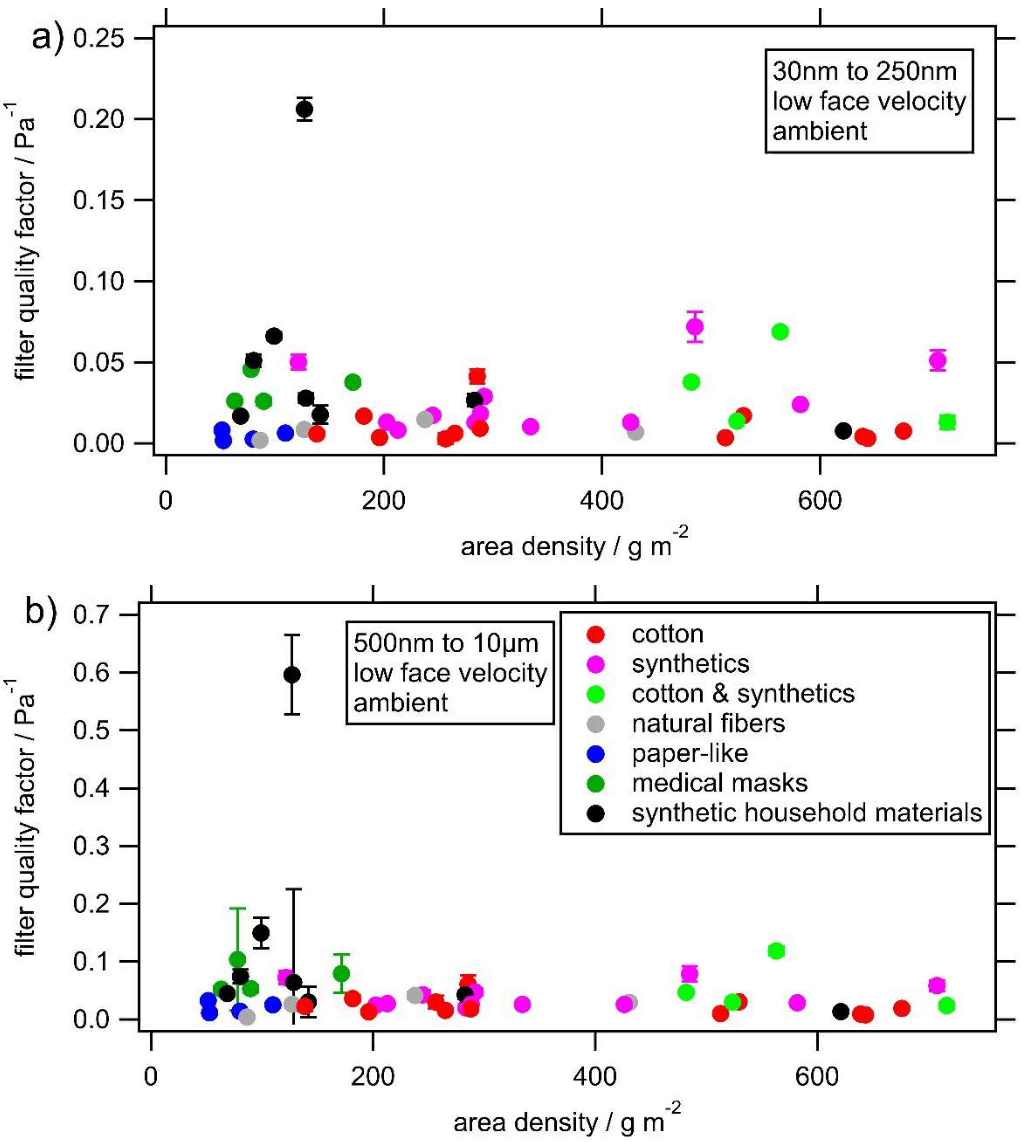

Figure S26: Filter quality factor versus area density for a) small and b) large particles, color-coded for material type. Ambient aerosol, measured with the *SMPS/OPC setup*, low face velocity.

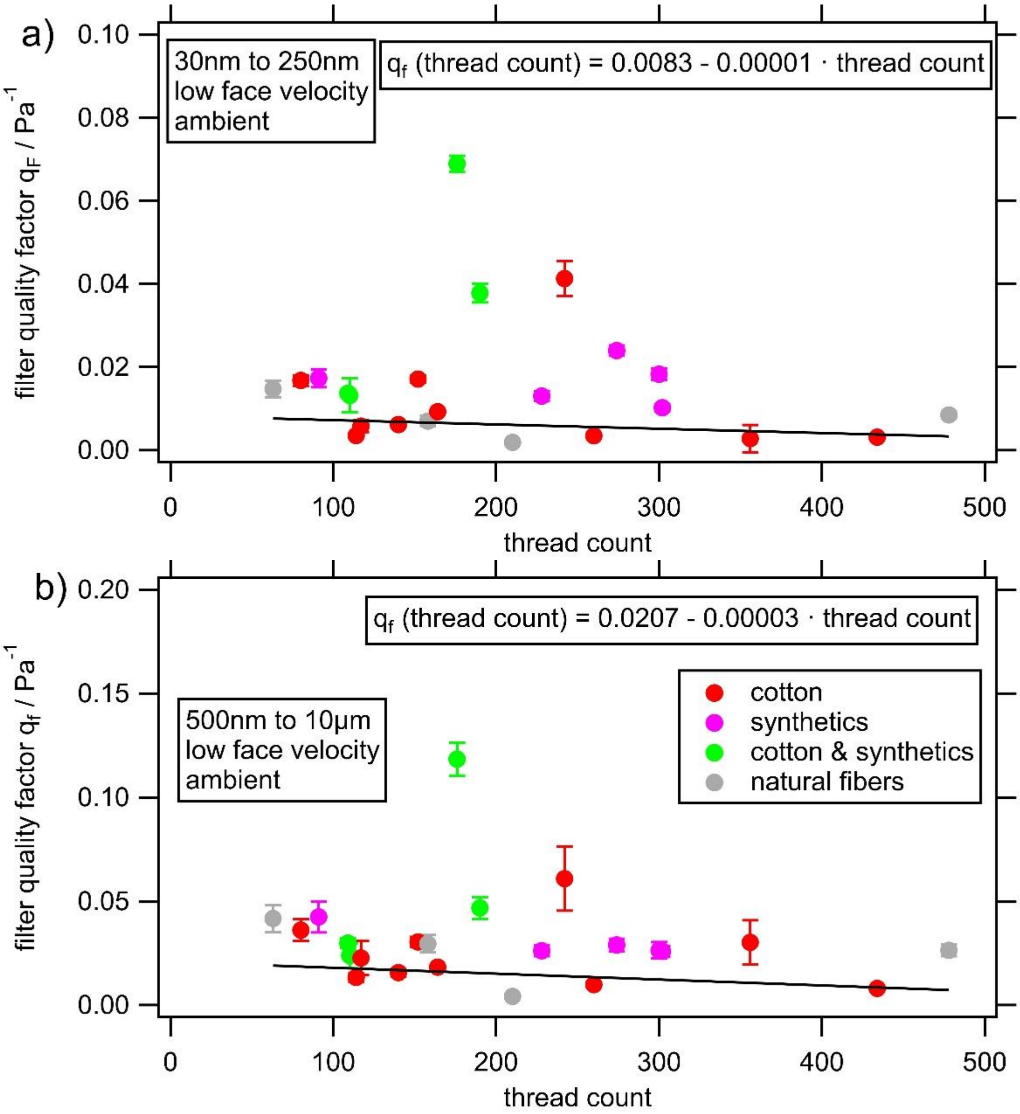

Figure S27: Filter quality factor versus thread count for a) small and b) large particles, color-coded for material type. Ambient aerosol, measured with the *SMPS/OPC setup*, low face velocity.

S3: Estimate of "leak separation efficiency"

To investigate the dependency of total filtration efficiency of leaking samples as a function of particle size further, i.e., to determine how well particles follow the flow through the leaks, we used the measurements at the leaking samples performed at the same pressure drop as those at the leak-free samples. Assuming that the face velocity through the sample material is the same as for the leak-free sample under this condition, we calculated the fraction of the total flow through the sample material f_{sample} and the fraction through the holes f_{leak}. Using the measured filtration efficiencies for the leak-free sample $FE_{leak\text{-}free}$ and for the leaking sample FE_{leak} we calculated the separation efficiency SE_{leak} of the leak:

$$FE_{leak} = FE_{leak-free} \cdot f_{sample} + SE_{leak} \cdot f_{leak} \qquad [S4]$$

$$SE_{leak} = \frac{FE_{leak} - FE_{leak-free} \cdot f_{sample}}{f_{leak}} \qquad [S5]$$

The leak separation efficiency, which reflects which fraction of the respective particles is lost from the leak flow and has to pass through the filter material, calculated for the individual particle diameters and for both samples is presented in Fig. S28. Several assumptions are integrated in these calculations, like the assumption that the occurrence of leaks does not influence the flow through the sample material around the leak, for which we do not have quantitative information of their validity. Therefore, we did not include error bars with the data points and treat this figure more qualitatively. Still these results support the assumption that for smaller particles (d_p≤2.5 µm), leak separation efficiency is close to zero, i.e., most particles follow the air flow through the leaks. For larger particles, this is not completely the case anymore and particles tend to be lost from the leak flow with increasing separation efficiency for increasing particle diameter and have to pass through the filter material.

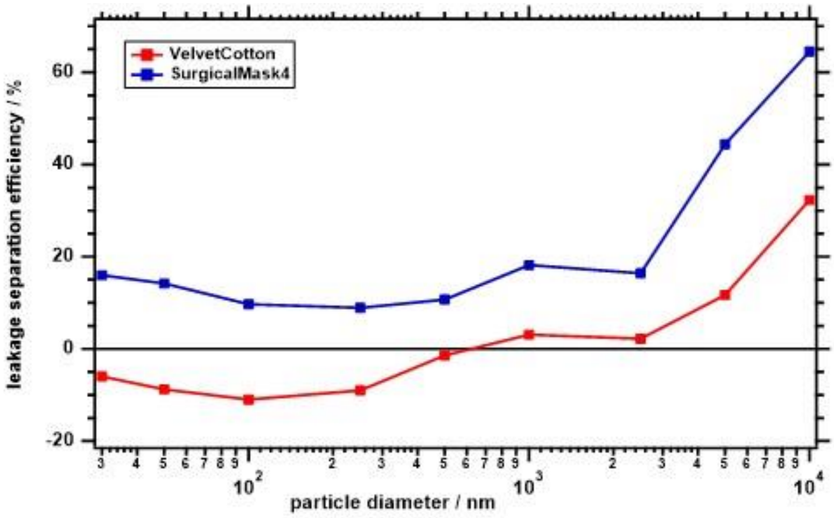

Fig. S28: Estimated separation efficiency for the leak flow as a function of particle size for velvet cotton (red) and surgical mask (blue) samples versus particle diameter.

References

Levin, E. J. T., G. R. McMeeking, C. M. Carrico, L. E. Mack, S. M. Kreidenweis, C. E. Wold, H. Moosmüller, W. P. Arnott, W. M. Hao, J. L. Collett Jr., and W. C. Malm. 2010. Biomass burning smoke aerosol properties measured during Fire Laboratory at Missoula Experiments (FLAME). *Journal of Geophysical Research: Atmospheres* 115:D18210. doi:10.1029/2009jd013601.

Seinfeld, J. H., and S. N. Pandis. 2006. *Atmospheric chemistry and physics: From air pollution to climate change*. 2nd ed. New York: John Wiley & Sons.

Tang, I. N. 1996. Chemical and size effects of hygroscopic aerosols on light scattering coefficients. *Journal of Geophysical Research: Atmospheres* 101:19245-50, doi:10.1029/96JD03003.

Levin, E. J. T., McMeeking, G. R., Carrico, C. M., Mack, L. E., Kreidenweis, S. M., Wold, C. E., Moosmüller, H., Arnott, W. P., Hao, W. M., Collett Jr., J. L., and Malm, W. C.: Biomass burning smoke aerosol properties measured during Fire Laboratory at Missoula Experiments (FLAME), Journal of Geophysical Research: Atmospheres, 115, D18210, 10.1029/2009jd013601, 2010.

Seinfeld, J. H., and Pandis, S. N.: Atmospheric Chemistry and Physics: From Air Pollution to Climate Change, 2nd ed., John Wiley & Sons, Inc., New York, 2006.

Tang, I. N.: Chemical and size effects of hygroscopic aerosols on light scattering coefficients, Journal of Geophysical Research: Atmospheres, 101, 19245-19250, 10.1029/96JD03003, 1996.

Vetter, T.: Berechnung der Mie-Streufunktionen zur Kalibrierung optischer Partikelzähler, diploma thesis, Institut für Physik der Atmosphäre, Johannes Gutenberg-Universität Mainz und Abteilung Wolkenphysik und -chemie, Max-Planck-Institut für Chemie Mainz, Johannes Gutenberg-Universität Mainz, Mainz, 2004.